

# Introduction to the Invariant Spin Field and Update on Simulations with Polarized Protons at HERA-p

M.Vogt, D.P.Barber and G.H.Hoffstätter

May 15, 1998

## Abstract

This report has mainly two aims: 1) introduce the concept of the invariant spin field to accelerator physicists (section 2). 2) give an update on the status of the “polarized protons at HERA project” including studies on the pre-accelerator (section 3) chain and recent simulations for crossing the strongest depolarizing resonance directly below the working energy of 820 GeV (section 4).

## Contents

<b>1</b>	<b>General Introduction</b>	<b>2</b>
<b>2</b>	<b>Introduction to Spin Dynamics in Circular Accelerators</b>	<b>2</b>
2.1	The T-BMT-Equation . . . . .	3
2.2	The Invariant Spin Field . . . . .	4
2.2.1	The Static Polarization Limit . . . . .	6
2.3	Spin Orbit Depolarizing Resonances . . . . .	8
2.4	Siberian Snakes . . . . .	12
2.5	The Acceleration Process . . . . .	17
<b>3</b>	<b>The HERA-p pre-accelerator chain</b>	<b>20</b>
3.1	The $H^-$ source . . . . .	21
3.2	RFQ, LEBT, LINAC-III and transfer lines . . . . .	21
3.3	DESY-III . . . . .	22
3.4	PETRA-p . . . . .	22
3.5	Polarimeters . . . . .	23
<b>4</b>	<b>Conservation of Polarization on the Energy Ramp</b>	<b>23</b>
<b>5</b>	<b>Conclusion</b>	<b>37</b>

# 1 General Introduction

Electron/positron polarization has become a routine aspect of operation at HERA, with the 27.5 GeV  $e^+$  beam with usually 50—70% longitudinal polarization being scattered on the internal gas target at the HERMES experiment. Due to the great success of the HERMES experiment other collaborations (ZEUS, H1, HERA-N) want to use a polarized 820 GeV proton beam to do  $e/p$ -scattering with the full HERA-kinematics. Not only can the deep inelastic spin structure functions  $g_1$ ,  $g_2$  be measured but also di-jet events, photo production, vector meson production, diffractive processes and many other processes are expected to have measurable asymmetries once reasonable polarization *and* integrated luminosity can be provided [1].

Protons, in contrast to electrons, cannot be polarized at high energy yet. Hence they must be created in a polarized source and then accelerated through the whole pre-accelerator chain up to 820 GeV in HERA-p. Not only must the problem of low intensity  $H^-$  sources be overcome but also the many thousand depolarizing resonances that act on the beam at ramp time [2].

In the past several machines have successfully accelerated polarized protons but all of them were low or medium energy machines. The highest energy reached so far is almost 25 GeV for the AGS at BNL [15]. In the near future RHIC at BNL will come into operation and in the year 2000 the first polarized proton runs are planned to start at  $2 \times 250$  GeV. But there are no other approved plans for high energy accelerators for polarized proton operation. The customary theories of depolarization are not likely to work in the high energy regime. They can only make predictions about the polarization losses as long as the strong spin perturbing energy regions (around “depolarizing resonances”) are well separated. At high energy these regions become fairly wide. Therefore a new more complete model of polarization in circular accelerators has to be applied.

## 2 Introduction to Spin Dynamics in Circular Accelerators

The motion of charged particles in an accelerator is determined by the electromagnetic fields. If the charged particles have non-zero spin, they have a magnetic dipole moment so that the spin of a particle moving in electromagnetic fields will precess according to the T-BMT equation (see section 2.1). At accelerator energies the Stern-Gerlach forces can be neglected. Thus spin has hardly any effect on the orbital motion, but spin dynamics itself is driven by the changing fields experienced on a particle trajectory.

In principle spin is a quantum mechanical property, but since we are interested in ensemble averages only, since a typical proton bunch at HERA consists of  $10^{11}$  particles and since the typical scales in phase space are large compared to  $\hbar$ , we can treat most aspects of spin motion classically — with two exceptions. First, synchrotron radiation is emitted discontinuously *and* the spin flip amplitude for the radiation process is non-zero. This effect can be neglected for proton beams in all existing accelerators. Second, the gyro-magnetic anomaly ( $G = \frac{g-2}{2} \approx 1.79$  for protons) appears in the equations of motion. This quantity can only be computed using quantum field theory.

With the above restrictions we will from now on treat spins classically, i.e. a classical spin  $\hat{S} \in \mathbb{S}_3$  is a unit vector in 3 dimensional space. A fermionic particle with mass  $m$ , electromagnetic charge  $q$ , gyro-magnetic factor  $g$  and spin  $\hat{S}$  has a magnetic moment  $\vec{\mu}_{\hat{S}} = \frac{q}{2m} g \frac{\hbar}{2} \hat{S}$ .

Beam polarization  $\vec{P}$  is the ensemble average of Pauli matrix expectation values. In the classical limit we have

$$\vec{P}(l) = \langle \hat{S} \rangle_{\text{ensemble}} = \int_{\mathbb{R}^6} \vec{P}_{\text{loc}}(\vec{z}, l) \rho(\vec{z}, l) d^6z \quad , \quad (1)$$

with  $\rho$  being the orbital phase space density normalized to 1 and  $\vec{P}_{\text{loc}}(\vec{z}, l)$  being the polarization at  $(\vec{z}, l)$ .

## 2.1 The T-BMT-Equation

The Lorentz force in a purely magnetic lattice element can be written in the lab frame as

$$\frac{d\vec{p}(t)}{dt} = \frac{-q}{m\gamma} \vec{B}(\vec{r}(t)) \times \vec{p}(t) \quad , \quad (2)$$

where  $\vec{B}(\vec{r}(t))$  indicates that the field has to be evaluated locally at the trajectory of the particle in configuration space. Therefore, after an infinitesimally short time interval  $dt$  the momentum of the particle has changed by  $\frac{\|d\vec{p}\|}{\|\vec{p}\|} = \frac{|q|}{m\gamma} \|\vec{B}\| dt \equiv \delta_{\text{orb}}$ , when  $\vec{B} \perp \vec{p}$ . When restricting to transverse magnetic fields the T-BMT equation [3] looks similar

$$\frac{d\hat{S}(t)}{dt} = \frac{-q}{m\gamma} (G\gamma + 1) \vec{B}_{\perp}(\vec{r}(t), \vec{p}(t)) \times \hat{S}(t) \quad , \quad (3)$$

where  $G = \frac{g-2}{2} = 1.79$  is the gyromagnetic anomaly of the proton and  $\vec{B}_{\perp}(\vec{r}(t), \vec{p}(t))$  indicates that  $\vec{B}_{\perp} \equiv \vec{B} - \vec{p} \frac{\vec{B} \cdot \vec{p}}{\|\vec{p}\|^2}$  is to be evaluated at  $(\vec{r}(t), \vec{p}(t))$ . In analogy to the Lorentz force case the infinitesimal spin precession will be  $\|d\hat{S}\| = (G\gamma + 1) \frac{|q|}{m\gamma} \|\vec{B}_{\perp}\| dt \equiv (G\gamma + 1) \delta_{\text{orb}}$ . Hence every transverse magnetic field that acts on the orbit acts on the spin  $(G\gamma + 1)$  times as much! In a (purely fictitious) ring with only constant vertical magnetic fields i.e. with only horizontal bends, after one revolution around the ring all spins will have precessed around the vertical axis by  $2\pi G\gamma$  plus one additional full revolution from the particle orbit ( $\rightarrow G\gamma + 1$ ). We will refer to  $G\gamma$  as the “spin enhancement factor”. From (3) we see that the spin precession due to a transverse magnetic field is energy independent for  $\gamma \gg 1$ .

In the presence of more general electromagnetic fields the T-BMT equation reads

$$\begin{aligned} \frac{d\hat{S}(t)}{dt} &= \tilde{\tilde{\Omega}}(\vec{r}(t), \vec{p}(t)) \times \hat{S}(t) \quad , \\ \tilde{\tilde{\Omega}}(\vec{r}(t), \vec{p}(t)) &\equiv \frac{-q}{m\gamma} \left[ (1 + G\gamma) \vec{B}_{\perp} + (1 + G) \vec{B}_{\parallel} + \left( G + \frac{1}{1 + \gamma} \right) \frac{\vec{E} \times \vec{p}}{m} \right] \quad . \end{aligned} \quad (4)$$

With respect to accelerator coordinates the T-BMT equation finally becomes

$$\frac{d\hat{S}(l)}{dl} = \left[ \left( \frac{dt}{dl} \right) \tilde{\tilde{\Omega}}(\vec{z}(l), l) - \vec{\kappa}(l) \times \hat{u}_l(l) \right] \times \hat{S}(l) \equiv \vec{\Omega}(\vec{z}(l), l) \times \hat{S}(l) \quad , \quad (5)$$

where  $l$  is the arc length,  $\vec{z} = (x, x', y, y', \tau, \eta)$  is the 6 dimensional phase space vector of the particle in Hamiltonian accelerator coordinates,  $\hat{u}_l$  is the longitudinal unit vector and  $\vec{\kappa}$  is the vector of curvature of the closed orbit. The orbital motion  $\vec{z}(l)$  is assumed to be known already.

Note that inside  $\vec{\Omega}$  the extra rotation from the closed orbit, that was still in  $\vec{\tilde{\Omega}}$ , has been subtracted ( $G\gamma + 1 \rightarrow G\gamma$ ).

From the structure of all three versions of the T-BMT equation we can conclude that length of a spin is conserved as well as the initial angle between two spins that travel through the same field configuration.

$$\angle(\hat{S}_1(l), \hat{S}_2(l)) = \angle(\hat{S}_1(l_0), \hat{S}_2(l_0)) \quad \forall l \quad ; \quad \|\hat{S}(l)\| = \text{const.} \quad (6)$$

Hence the flow of (5) must be an orthogonal map,

$$\hat{S}_f = \underline{R}(l_f, l_i; \vec{z}_i) \hat{S}_i \quad , \quad (7)$$

with  $\underline{R} \in \mathbf{SO}(3)$ . Since (5) is driven by the orbital motion of the particle, the flow in (7) explicitly contains the initial phase space point  $\vec{z}_i$  and implicitly includes the full trajectory  $\vec{z}(l), l_i \leq l \leq l_f$ .

## 2.2 The Invariant Spin Field

There are many mathematical tools (Twiss functions, emittances (= “actions”), phase advances (= “angles”), etc.) to describe the orbital motion in accelerators. This section gives an introduction to a powerful mathematical construct to describe spin motion in circular accelerators. If we restrict ourselves to *linear* orbit motion, then the orbit flow will be a *linear* symplectic map

$$\vec{z}_f = \underline{T}(l_f, l_i) \vec{z}_i \quad , \quad (8)$$

and all particles that have a set of orbital amplitudes  $(\varepsilon_1, \varepsilon_2, \varepsilon_3) \equiv 2\vec{J}$  will stay on a torus independent of  $l$ . In this paper “emittance” always refers to the orbital amplitude of a particle moving on a phase space torus. But we often state it in units of ‘ $\sigma$ ’ where  $\sigma$  is an rms. action of the beam. The solution of the equations of motion can be written as

$$\vec{J}_f = \vec{J}_i \quad , \quad \vec{\Psi}_f = \vec{\Psi}_i + \frac{2\pi(l_f - l_i)}{L} \vec{Q} \quad . \quad (9)$$

The shape of this torus, transformed to standard phase space coordinates  $(x, x', y, y', \tau, \eta)$ , will usually change during one revolution but it is periodic with period  $L$ . If the machine is totally decoupled, the Cartesian transformation of the normal torus will be the direct product of 3 ellipses in the  $x$ - $x'$ ,  $y$ - $y'$  and  $\tau$ - $\eta$  plane. This normal torus is an invariant manifold under the flow (8).

The spin is transported (7) by  $\underline{R}(l_f, l_i; \vec{z}_i)$  which is a function of the phase space. The  $\hat{n}$ -axis  $\hat{n} : \mathbb{R}^6 \times [0, L[ \rightarrow \mathbb{S}_3$  on an invariant torus  $\vec{z}(\vec{J}, \vec{\Psi}(l))$  with  $\vec{J} = \text{const.}$  is defined as a unit length invariant spin field under the flow (7) and (8) for *constant* parameters, in particular for a constant reference energy.

$$\hat{n}(\vec{z}_f, l_f) = \underline{R}(l_f, l_i; \vec{z}_i) \hat{n}(\vec{z}_i, l_i) \quad . \quad (10)$$

If it exists, it can be periodically extended without discontinuities,

$$\hat{n}(\vec{z}, l + L) = \hat{n}(\vec{z}, l) \quad . \quad (11)$$

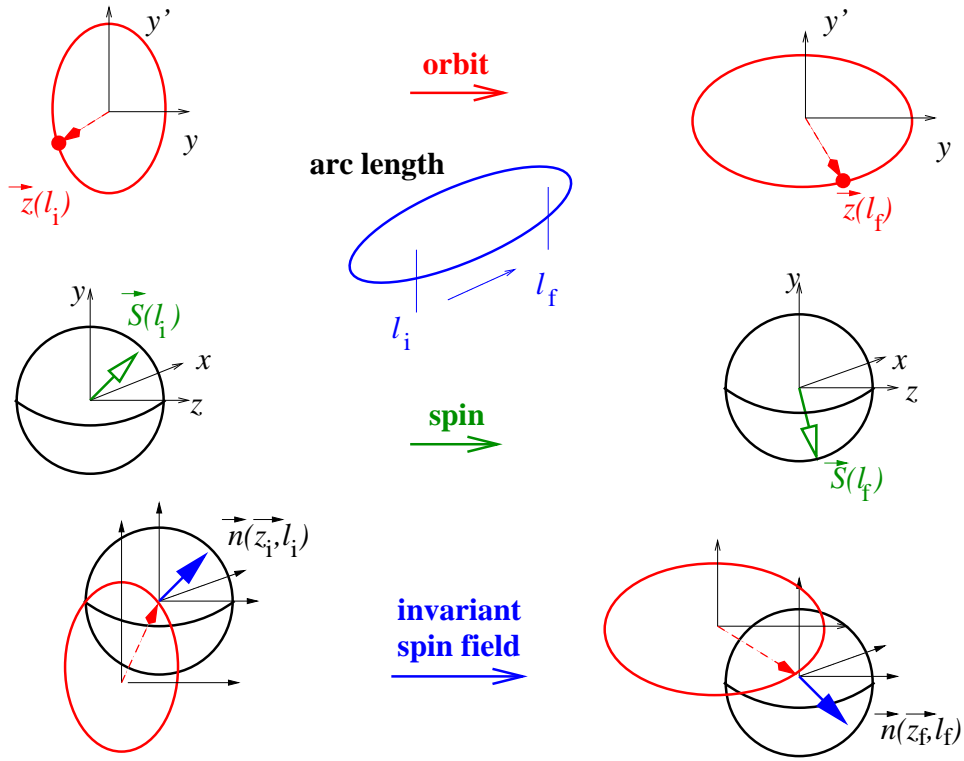


Figure 1: During particle motion from  $l_i$  to  $l_f$  the orbital phase space coordinates (top) stay on ellipse of constant area, the spin unit vector stays on a unit sphere, and the invariant spin field is transported from the sphere attached to the initial phase space vector to the sphere attached to the final phase space vector

Hence on a given trajectory  $\vec{z}(l) = \underline{T}(l, l_0)\vec{z}_0$  with constant parameters the  $\hat{n}$ -axis is a special solution of (5)

$$\frac{d\hat{n}(\vec{z}(l), l)}{dl} = \vec{\Omega}(\vec{z}(l), l) \times \hat{n}(\vec{z}(l), l) , \quad (12)$$

with periodic boundary conditions. That is why  $\hat{n}$  is often called “periodic” solution, although the periodicity (11) of a single  $\hat{n}$ -axis is visible on a synchro-betatron trajectory only if all orbital tunes are integers. More generally one could say if there are integers  $m, m_x, m_y, m_{\text{sync}}$  such that  $mQ_i = m_i$  ( $i = x, y, \text{sync}$ ) then  $\hat{n}(\vec{z}, l)$  is eigenvector of the  $m$ -turn spin map for all  $\vec{z}$  or  $\hat{n}(\vec{z}(l + mL), l + mL) = \hat{n}(\vec{z}(l), l)$ .

The restriction of  $\hat{n}(\vec{z}, l)$  to the closed orbit is the eigenvector with eigenvalue 1 of the one-turn spin map on the closed orbit,

$$\hat{n}(\vec{0}, l) \equiv \hat{n}_0(l) = \hat{n}_0(l + L) = \underline{R}(l + L, l; \vec{0})\hat{n}_0(l) . \quad (13)$$

For a flat ring with no Siberian Snakes (see section 2.4), no solenoids, and no closed orbit perturbations the  $\hat{n}_0$ -axis is vertical all over the ring and for the fictitious ring with no quadrupoles, introduced as an example in section 2.1,  $\hat{n}(\vec{z})$  is independent of  $\vec{z}$  and equal to  $\hat{n}_0$ . Note that the  $\hat{n}$ -axis has an arbitrary sign, since it is defined as periodic unit vector field of the extended orbital phase space that is compatible with the T-BMT flow. The spin on the other hand is a dynamical variable itself and determined by an initial value problem  $\frac{d}{dl}\hat{S} = \vec{\Omega} \times \hat{S}$  and  $\hat{S}(l = 0) = \hat{S}_0$ .

Figure 1 depicts the mapping of an initial to a final state (left to right) for the orbital phase space (top), a simple spin (middle) and an  $\hat{n}$ -axis (bottom). The orbital position moves along

ellipses of constant area, the spin moves on the unit sphere and the  $\hat{n}$ -axis is transported from one unit sphere attached to the initial phase space point to another unit sphere attached to the final phase space point.

From (6) we conclude that, as long as the reference energy is fixed, the motion of an arbitrary spin given at  $\hat{S}_i = \hat{S}(\vec{z}_i, l_i)$  is a rotation on a cone with fixed polar angle around a vector  $\hat{n}(\vec{z}(l; \vec{z}_i), l)$ . This vector  $\hat{n}$  is a function of the extended orbital phase space only and has to be evaluated on the trajectory of the particle. The invariant

$$J_s \equiv \hat{S}(l; \vec{z}_i, \hat{S}_i) \cdot \hat{n}(\vec{z}(l; \vec{z}_i), l) = \text{const.} = \hat{S}_i \cdot \hat{n}(\vec{z}_i, l_i) \quad (14)$$

is called the spin action [4].

We can then find a rotating coordinate system [4]  $(\hat{u}_1(\vec{z}, l), \hat{n}(\vec{z}, l), \hat{u}_3(\vec{z}, l))$  such that spin motion in these coordinates is just

$$\hat{S}(l) = \left( \sqrt{1 - J_s^2} \sin[\nu_s(\vec{J}) \frac{2\pi l}{L} + \phi_0], J_s, \sqrt{1 - J_s^2} \cos[\nu_s(\vec{J}) \frac{2\pi l}{L} + \phi_0] \right) . \quad (15)$$

The function  $\nu_s(\vec{J})$  is called the amplitude dependent spin tune. Normally it depends on the reference energy  $\nu_s(\vec{J}) = \nu_s(\vec{J}; E_0)$  but with a few exceptions we will suppress this dependency since in a large fraction of this paper we assume the reference energy to be constant. In a flat machine without snakes and solenoids the spin tune on the unperturbed design orbit is just the spin enhancement factor

$$\nu_0^{\text{flat, perfect}} \equiv \nu_s^{\text{flat, perfect}}(\vec{0}) = G\gamma . \quad (16)$$

The two additional unit vector fields  $\hat{u}_{(1,2)} : \mathbb{R}^6 \times [0, L[ \rightarrow \mathbb{S}_3$ , can be periodically extended without discontinuity  $\hat{u}_{(1,2)}(\vec{z}, l + L) = \hat{u}_{(1,2)}(\vec{z}, l)$  but they are *not* solutions of the T-BMT equation. In general  $\hat{u}_{(1,2)}$  are difficult to construct explicitly.

In the case where we neglect all but one plane in phase space the phase space points of successive revolutions  $(\vec{z}(l_j))_{j \in \mathbb{N}} = \vec{z}(l_0), \vec{z}(l_0 + L), \dots$  are on one ellipse with  $J = \text{const.}$ ,  $\Psi_j = \Psi_0 + jQ$  rather than on a torus with  $\vec{J} = \text{const.}$ ,  $\vec{\Psi}_j = \vec{\Psi}_0 + j\vec{Q}$ . As long as the  $\hat{n}$ -axis is a smooth function on a given ellipse, the image of the ellipse under  $\hat{n}$  will be a closed curve on the unit sphere  $\mathbb{S}_3$ . Figure 2 shows such a closed curve computed with the spin code `SPRINT` [6]. The  $\hat{n}$ -axis was computed for one single point  $\vec{z}_0$  and then just transported by tracking for 1000 turns. In figure 2 the calculations were performed for the HERA-p 1996 luminosity lattice setup at 801.5 GeV. The emittance was  $64\pi$  mm mrad which is approximately the  $4\sigma$  vertical emittance. The locus of the  $\hat{n}$ -axis in this example is a closed curve as predicted, but with a large angular spread and multiply curled up. The complex structure of the curve in this almost arbitrary example is an indication for the complexity of spin motion at high energy.

For electrons with radiative polarization and depolarization mechanisms (and for protons once noise, intra beam scattering, etc. is introduced) the  $\hat{n}$ -axis turns out to be (up to some small deviations [7]) the equilibrium polarization axis. In the quantum mechanical picture of polarization the  $\hat{n}$ -axis is a function that commutes with all spin operators and defines the local quantization axis for which the density matrix of spin states becomes diagonal. Thus we can treat spin states as being eigenstates of  $\vec{\sigma} \cdot \hat{n}(\vec{z}, l)$  with  $\vec{\sigma}$  being the vector of Pauli matrices.

### 2.2.1 The Static Polarization Limit

In this section the position in arc length  $l$  will be fixed and therefore omitted in all equations for brevity.

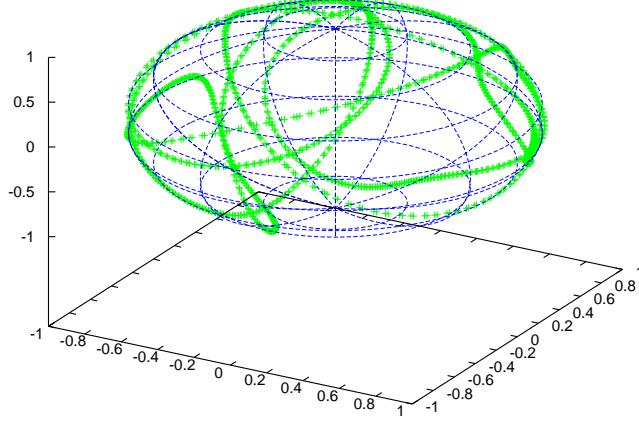


Figure 2: The  $\hat{n}$ -axis for HERA-p with a special Siberian Snake arrangement at 801.5 GeV on an invariant phase space ellipse with  $64\pi$  mm mrad vertical emittance plotted on the unit sphere.

The local polarization  $\vec{P}_{\text{loc}}$  at a given phase space point  $\vec{z}$  is given by

$$\vec{P}_{\text{loc}}(\vec{z}) = P_{\text{dyn}}(\vec{z})\hat{n}(\vec{z}) , \quad (17)$$

where the dynamical polarization  $P_{\text{dyn}}$  is the average over spins  $\hat{S}_k$  at  $\vec{z}$

$$P_{\text{dyn}} = \langle \hat{S}_k(\vec{z}) \cdot \hat{n}(\vec{z}) \rangle_k = \langle J_{s,k}(\vec{z}) \rangle_k , \quad (18)$$

where  $J_{s,k}(\vec{z})$  is the spin action of the  $k$ -th particle at  $\vec{z}$  with respect to  $\hat{n}(\vec{z})$ . If spin motion is well behaved at ramp time, then  $P_{\text{dyn}}$  is a property of the beam that is fixed by more or less good matching at injection. If spin motion is strongly perturbed (“resonance crossing”) on the ramp,  $P_{\text{dyn}}$  can change. As an example take all spins parallel to their local  $\hat{n}$ -axis at injection, then  $P_{\text{dyn}}$  is just 1 if there are no losses on the ramp. The total polarization that can be measured by experiments is therefore

$$\vec{P}_{\text{tot}} = \int_{\mathbb{R}^6} \rho(\vec{z}) P_{\text{dyn}}(\vec{z}) \hat{n}(\vec{z}) d^6 \vec{z} . \quad (19)$$

Now we will transform to action-angle variables ( $\vec{z} \rightarrow (\vec{J}, \vec{\Psi})$ ). In particular we will make the following assumptions

- $\frac{\partial \rho}{\partial \vec{\Psi}} \approx \vec{0}$ . In a real accelerator small non-linearities of the orbital motion will smear out small inhomogeneities on the torus (filamentation). Filamentation generally averages away the  $\vec{\Psi}$  dependence of  $\rho$  even in a regime where the nonlinearities are so weak that the orbital motion is still integrable to a good approximation.
- $\frac{\partial P_{\text{dyn}}}{\partial \vec{\Psi}} \approx \vec{0}$ . Spins on the same torus are supposed to have the same averaged history.

If these assumptions are applicable at least to some extent, then in the worst case we can replace  $\rho$  by  $\langle \rho \rangle_{\vec{\Psi}}$  and  $P_{\text{dyn}}$  by  $\langle P_{\text{dyn}} \rangle_{\vec{\Psi}}$  so that the following statements remain approximately correct. Defining the angle averaged  $\hat{n}$ -axis (for non vanishing norm!)

$$\hat{u}_{\langle n \rangle}(\vec{J}) \equiv \frac{\langle \hat{n}(\vec{J}, \vec{\Psi}) \rangle_{\vec{\Psi}}}{\left\| \langle \hat{n}(\vec{J}, \vec{\Psi}) \rangle_{\vec{\Psi}} \right\|} , \quad (20)$$

and the static polarization limit

$$P_{\text{lim}}(\vec{J}) \equiv \left\langle \hat{u}_{\langle n \rangle}(\vec{J}) \cdot \hat{n}(\vec{J}, \vec{\Psi}) \right\rangle_{\vec{\Psi}} , \quad (21)$$

we obtain the following decomposition

$$\vec{P}_{\text{tot}} = \int_{\mathbb{R}_+^3} \tilde{\rho}(\vec{J}) P_{\text{dyn}}(\vec{J}) P_{\text{lim}}(\vec{J}) \hat{u}_{\langle n \rangle}(\vec{J}) d^3 \vec{J} , \quad (22)$$

where all normalization and transformation factors have been absorbed into  $\tilde{\rho}$ . Using (22) we have factorized the observable beam polarization into a dynamic, “history dependent” part ( $\tilde{\rho}$  and  $P_{\text{dyn}}$ ) and static part ( $\hat{u}_{\langle n \rangle}$  and  $P_{\text{lim}}$ ). The static part only depends on the emittances, the energy, and the structure of the lattice. If the T-BMT equation is linear in the orbit, it can be shown that in a flat ring without solenoids, without closed orbit distortions, and without snakes or with snakes that make  $\hat{n}_0$  vertical  $\hat{u}_{\langle n \rangle}$  is independent of  $\vec{J}$  and parallel to  $\pm \hat{n}_0$ . Hence the total polarization is then  $\pm \hat{n}_0 \int \tilde{\rho}(\vec{J}) P_{\text{dyn}}(\vec{J}) P_{\text{lim}}(\vec{J}) d^3 \vec{J}$ .

The linear orbital properties of the beam can be described by the  $\beta$ -functions, and the emittances. The  $\beta$ -functions are functions of the lattice only, but the emittances are intrinsic beam properties. They are adiabatic invariants and depend on the beam history. In the case of spin motion we have the lattice function  $P_{\text{lim}}(\vec{J}) \hat{u}_{\langle n \rangle}(\vec{J})$  that can to some extent be regarded as the “spin- $\beta$ -function” and the beam property  $P_{\text{dyn}}(\vec{J})$  that could be called the “spin emittance” of the beam with the exception that a large dynamical polarization is considered advantageous whereas a large orbital emittance is normally considered disadvantageous.

A more geometrical property of the  $\hat{n}$ -axis that is somehow complementary to  $P_{\text{lim}}$  is the averaged polar opening angle of the invariant spin field on a given torus

$$\alpha(\vec{J}) = \left\langle \angle \left( \hat{u}_{\langle n \rangle}(\vec{J}), \hat{n}(\vec{J}, \vec{\Psi}) \right) \right\rangle_{\vec{\Psi}} . \quad (23)$$

It represents the directional spread of the invariant spin field. For small opening angle  $\alpha \ll 1$  obviously  $P_{\text{lim}}(\vec{J}) \approx \cos \alpha(\vec{J})$  holds. In high energy storage rings like HERA-p the directional spread of the  $\hat{n}$ -axis can be reasonably large so that the upper limit of polarization  $P_{\text{lim}}$  is small. If for example the average opening angle is  $60^\circ$ , the total polarization can't be bigger than 50% and  $\alpha = \frac{\pi}{2}$  means zero polarization even if  $P_{\text{dyn}} = 1$  all over phase space!

## 2.3 Spin Orbit Depolarizing Resonances

Consider again a storage ring with only horizontal bending magnets. Then a spin will only experience vertical magnetic fields. From (3),(4) or (5) we conclude that all spins will rotate around the vertical axis ( $\hat{u}_y$ )  $G\gamma$  times per revolution and that  $\hat{n}(\vec{z}, l) \equiv \hat{n}_0(l) \equiv \hat{u}_y$ . Thus



if we manage to inject with a 100% vertical polarization, we will keep it forever disregarding the influence of noise, beam–beam effect, etc. Of course we know that every accelerator needs transverse focusing and, if we want a bunched beam we will have longitudinal focusing too. Hence the spin experiences radial magnetic fields depending on it's position in phase space. Synchrotron motion continuously changes  $G\gamma$  and feeds into the transverse motion via the dispersion. Also misalignments of the quadrupole positions leads to closed orbit perturbations. In particular the vertical betatron oscillations which are focused by *horizontal* magnetic fields make the spins tilt away from  $\hat{u}_y$ , but they would cancel out on the average unless a certain coherence condition between spin and orbital motion were fulfilled.

Figure 3 gives an example of how two spins, initially parallel but on different synchro–betatron trajectories, get rotated differently by the position dependent quadrupole fields of just two adjacent horizontally defocusing (QD) and focusing (QF) quadrupoles. The small residual

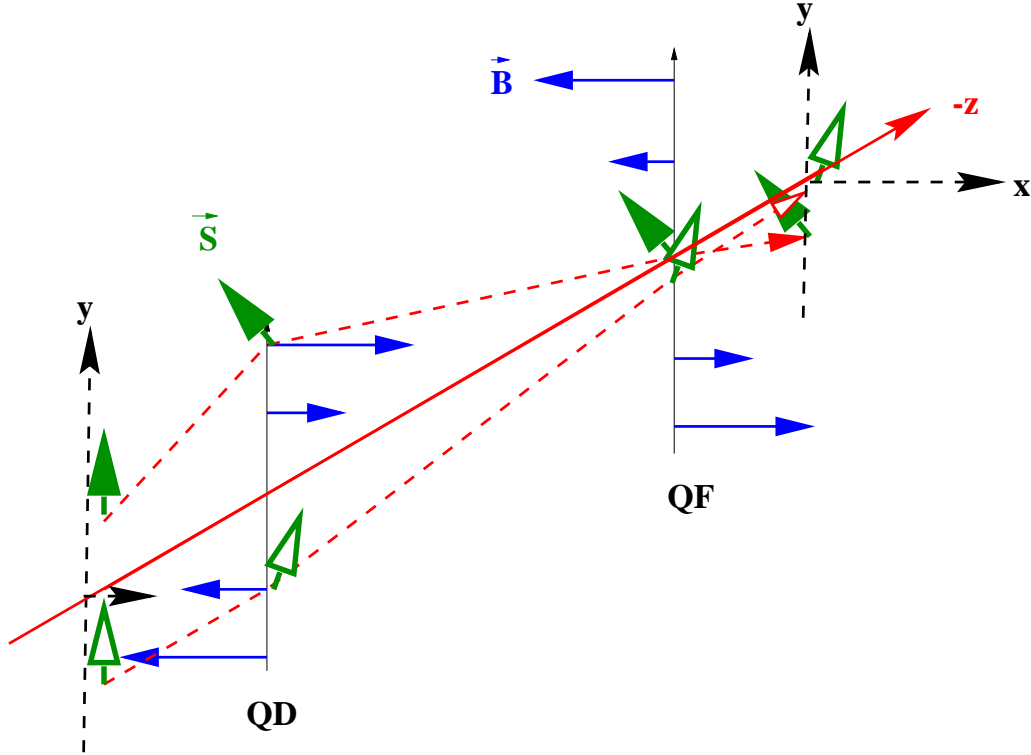


Figure 3: Spin perturbations form synchro betatron motion

rotations that come from the non–commutation of rotations around different axes add up and do harm if the spin and orbit motions are coherent, i.e. have the same dominant frequencies. If a spin on a certain torus is tilted away from the vertical on the average by one milliradian turn after turn, then after ca. 6000 revolutions it's locus has traversed the unit sphere. The actual precession axis changes with  $\vec{\Psi}$  on the torus and the average tilt angle is strongly dependent on the emittances.

The coherence condition for maximum spin perturbation is

$$\nu_s(E_0, \vec{J}) = k + k_x Q_x + k_y Q_y + k_{\text{sync}} Q_{\text{sync}} . \quad (24)$$

Resonances with  $k_x = k_y = k_{\text{sync}} = 0$  are called imperfection resonances. They are related to strong sensitivity to orbit distortions. If the spin tune is an integer, the unperturbed spin one

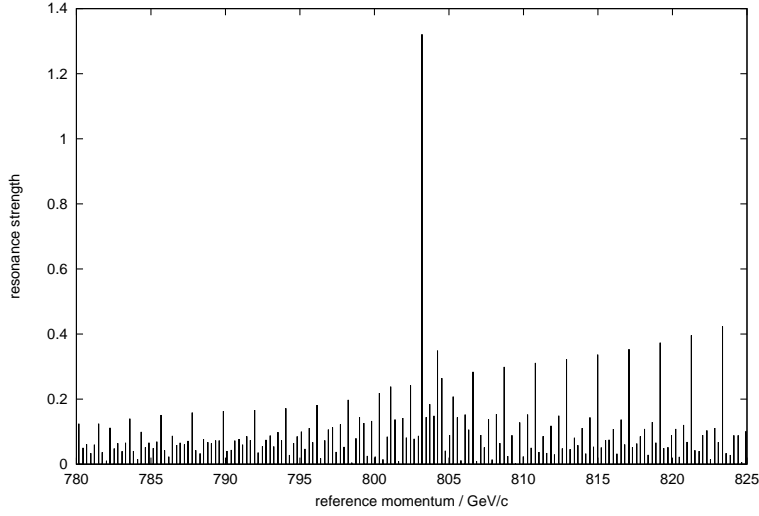


Figure 4: First order resonance strengths for “flat” HERA-p with  $16\pi$  mm mrad vertical emittance in the interval from 780 to 825 GeV

turn map  $\underline{R}$  is unity and therefore even tiny distortions of the ring dominate the spin motion. In a flat perfect machine ( $\nu_0 = G\gamma$ ) the energy difference between two adjacent imperfection resonances is  $\Delta E = \frac{m_p}{G} \approx 523$  MeV. Resonances with at least one of the  $k_x, k_y, k_{\text{sync}}$  non-zero are called intrinsic resonances of order  $|k_x| + |k_y| + |k_{\text{sync}}|$ . The disruptive effect of a first order intrinsic spin orbit depolarizing resonance is related to the perturbing T-BMT field defined by

$$\zeta_{\vec{J}}^{\hat{n}_0}(l) \equiv \omega_{\vec{J},1}^{(1)}(\vec{\Psi}(l), l) + i\omega_{\vec{J},3}^{(1)}(\vec{\Psi}(l), l) , \quad (25)$$

where  $\omega_{\vec{J},1}^{(1)}$  and  $\omega_{\vec{J},3}^{(1)}$  are those components of  $\vec{\omega}_{\vec{J}}(\vec{\Psi}, l) = \vec{\Omega}(\vec{z}, l) - \vec{\Omega}(\vec{0}, l)$  which are linear in  $\vec{z}$ , perpendicular to  $\hat{n}_0$  and are transformed to the reference system  $(\hat{m}_1(l), \hat{n}_0(l), \hat{m}_3(l))$ . This reference frame is  $L$ -periodic and for a machine with  $\hat{n}_0(l) \equiv \hat{u}_y$  it is just the machine frame  $(\hat{u}_x(l), \hat{u}_y(l), \hat{u}_z(l))$ , but generally needs an extra rotation to follow  $\hat{n}_0$ . The perturbing T-BMT field defines the rotation away from the  $\hat{n}_0$ -axis that a spin experiences on a synchro-betatron trajectory. The linear orbit  $\vec{z}(\vec{J}, \vec{\Psi}_0 + \frac{s\pi}{L}l\vec{Q})$ , is pseudo-periodic with the  $2\pi\vec{Q}$ -periodicity of the eigenvectors of the one turn map. If  $\vec{z}(l) = \sum_{\text{E.V.}} \vec{v}_k(l)a_k$ , then it transforms under the one turn map like  $\vec{z}(l+L) = \sum_{\text{E.V.}} \vec{v}_k(l+L)a_k = e^{i\frac{2\pi}{L}\text{diag}(\pm\vec{Q})} \sum_{\text{E.V.}} \vec{v}_k(l)a_k$ . The perturbing T-BMT field which is a function of  $(\vec{z}(l), l)$  can be decomposed into a Fourier series that contains the spectrum of  $\vec{z}$  only. If we restrict ourselves on linear orbit motion and linear  $\vec{\omega}$ , we obtain

$$\zeta_{\vec{J}}^{\hat{n}_0}(l) = \frac{2\pi}{L} \sum_{k=1}^{+\infty} \sum_{M \in \{x, y, \text{sync}\}} \left[ \epsilon_k^{M+}(\vec{J}) e^{i(k+Q_M)\frac{2\pi}{L}l} + \epsilon_k^{M-}(\vec{J}) e^{i(k-Q_M)\frac{2\pi}{L}l} \right] . \quad (26)$$

Note that each harmonic  $k$  is split into exactly two “side bands”  $k \pm Q_M$  per mode  $M$ . The first order resonance strength is

$$\epsilon_k^{M\pm}(\vec{J}) = \lim_{l \rightarrow \infty} \frac{1}{l} \frac{l}{2\pi} \int_0^l \zeta_{\vec{J}}^{\hat{n}_0}(l') e^{-i(k \pm Q_M)\frac{2\pi}{L}l'} dl' , \quad (27)$$

where the infinite domain is introduced due to the fact that  $(e^{-ik\frac{2\pi}{L}l})_{k \in \mathbb{Z}}$  is a complete orthogonal set of functions on  $[0, L]$  whereas  $(e^{-i[k \pm Q_M]\frac{2\pi}{L}l})_{k \in \mathbb{Z}, Q_M \in \mathbb{R}}$  is orthogonal on  $\mathbb{R}^+$  only and complete

only on the set of  $2\pi Q_M$  pseudo-periodic functions. The above definition includes an arbitrary complex phase due to the choice of the initial vectors ( $\hat{m}_1(0), \hat{n}_0(0), \hat{m}_3(0)$ ). Another method of computing the resonance strengths is given in [5]. In the case of a flat perfect ring without Siberian Snakes and without solenoids ( $\nu_0 = G\gamma$ ) and for sufficiently small orbital amplitudes ( $\nu_s(\vec{J}) \approx \nu_0$ ) the depolarizing resonances produce a discrete energy spectrum. If in addition the resonances are well separated, the opening angle  $\alpha$  is almost zero off-resonance and  $\frac{\pi}{2}$  exactly on a depolarizing resonance.

There is another aspect of  $\zeta$ . We can try to generalize  $\zeta_{\vec{J}}^{\hat{n}_0}(l)$  to  $\zeta_{\vec{J}}^{\hat{n}}(\vec{z}, l)$ , but we know that in any orthonormal based on the  $\hat{n}$ -axis and two other unit vectors, the spin is just precessing around  $\hat{n}$  with  $\hat{S} \cdot \hat{n} = \text{const}$  for constant energy. Hence  $\zeta_{\vec{J}}^{\hat{n}}(\vec{z}, l) = 0$  by definition which is another consistency constraint on the invariant spin field.

Usually the relation  $\epsilon_k^{M\pm} \propto \sqrt{J_M}$  holds for intrinsic resonances and the imperfection resonance strengths are approximately proportional to the rms. closed orbit distortion. The strongest first order resonances are related to the vertical motion and are driven by the periodic structure in the arcs [10]. Hence the approximate “super strong resonance condition” is

$$\nu_s(\vec{J}) = kP \pm Q_y \quad \text{and} \quad \nu_s(\vec{J}) \approx kPM \pm Q_y^{(\text{arcs})} \quad , \quad (28)$$

where  $P$  is the ring super period and  $M$  is the number of identical FODO-like cells of one super period, and  $2\pi Q_y^{(\text{arcs})}$  is the accumulated synchro-betatron phase advance of all regular arc sections. Figure 4 shows the intrinsic resonance strengths for a “flat” model of HERA-p in which the vertical bend sections have simply been switched of. The design orbit spin tune  $\nu_s(\vec{0})$  is then  $G\gamma$ . The resonance strengths are shown for a vertical emittance of  $16\pi$  mm mrad and the energy range is from 780 to 825 GeV. Note that there is one extremely strong resonance at  $G\gamma = 1535 - Q_y^{\text{fract}} = 1567 - Q_y^{\text{compl}}$  which corresponds to a momentum of about 803.2 GeV/c. The first order resonance strength (27) is often [10] generalized to the “ $\epsilon$ -function”

$$\epsilon(\vec{J}, \kappa) = \lim_{l \rightarrow \infty} \frac{1}{l} \frac{L}{2\pi} \int_0^l \zeta_{\vec{J}}^{\hat{n}_0}(l') e^{-i\kappa \frac{2\pi l'}{L}} dl' \quad (29)$$

by inserting the non-linear  $\vec{\omega}(\vec{z}, l)$  into (26), and/or using non-linear orbit motion. This is indicated by writing  $\tilde{\zeta}$  instead of  $\zeta$ . Whenever the spin tune  $\nu_s(E_0, \vec{J})$  is close to  $\kappa = k + k_x Q_x + k_y Q_y + k_{\text{sync}} Q_{\text{sync}}$  spin motion is maximally perturbed and the average opening angle  $\alpha(\vec{J})$  is increased.  $\epsilon(\vec{J}, \kappa)$  is then considered the strength of this perturbation. It has to be noted that for  $2\pi \vec{Q}$  pseudo-periodic orbital motion and linear  $\vec{\omega}$  the coefficients with  $|k_x| + |k_y| + |k_{\text{sync}}| > 1$  do not contribute to the Fourier expansion of  $\zeta_{\vec{J}}^{\hat{n}_0}(l)$ . Higher order tune harmonics in the spin motion arise from non-linear terms in  $\omega(\vec{z}, l)$ , partly from non-linear orbit motion  $\vec{z}(l)$  as the driving term of spin motion (which introduces orbital tune spread  $\vec{Q}(\vec{J})$  to the spectrum of  $\vec{\omega}$ ), but most of all from the intrinsic non-linearity of the spin map  $\underline{R}(l_f, l_i; \vec{z})$  with respect to the orbital phase space variables. The non-linearity of  $\underline{R}(l_f, l_i; \vec{z})$  is *not* included in  $\epsilon(\vec{J}, \kappa)$  in definition (29). But even for linear orbital motion *and* linear  $\vec{\omega}^{(1)}$  these non-linearities show up in the  $\hat{n}$ -axis.

There is an analytically solvable model with exactly one first order resonance in 2+1 dimensions called single resonance model [8], [9],

$$\frac{dJ}{dl} = 0 \quad ,$$

$$\begin{aligned}\frac{d\Psi}{dl} &= \frac{2\pi}{L}Q , \\ \vec{\Omega}(J, \Psi, l) &= \frac{2\pi}{L} (\epsilon(J) \sin \Psi , \nu_0 , \epsilon(J) \cos \Psi) .\end{aligned}\quad (30)$$

Setting

$$\Lambda = \sqrt{(\nu_0 - Q)^2 + \epsilon(J)^2} , \quad (31)$$

one can show that the  $\hat{n}$ -axis is given by

$$\hat{n}(J, \Psi, l) = \frac{\nu_0 - Q}{|\nu_0 - Q|} \frac{1}{\Lambda} (\epsilon(J) \sin \Psi , \nu_0 - Q , \epsilon(J) \cos \Psi) . \quad (32)$$

The amplitude dependent spin tune is

$$\nu(J) = \frac{\nu_0 - Q}{|\nu_0 - Q|} \Lambda + Q . \quad (33)$$

We immediately see that in this simple model the  $\hat{n}$ -axis is vertical far off-resonance where  $\nu_0 - Q$  is big and it tilts over to the horizontal plane at the resonance. Also the spin tune is linear in  $\nu_0$  for big  $\nu_0 - Q$  but makes a step from  $Q + \epsilon$  to  $Q - \epsilon$  at  $\nu_0 = Q$ .

For this model the ratio  $\frac{P_{\text{dyn}}(l=+\infty)}{P_{\text{dyn}}(l=-\infty)}$  after acceleration through a resonance at  $l = 0$  has been calculated by Froissart and Stora [11]. If the closed orbit spin tune is  $\nu_0 - Q = a \frac{2\pi l}{L}$  with the constant ‘‘ramp rate’’  $a$ , then

$$\frac{P_{\text{dyn}}(l = +\infty)}{P_{\text{dyn}}(l = -\infty)} = 2e^{-\pi \frac{\epsilon(J)^2}{2a}} - 1 . \quad (34)$$

In the asymptotic regions  $\epsilon^2 \ll a$  and  $\epsilon^2 \gg a$  the ratio in (34) is  $\approx 1$  and  $\approx -1$  respectively. In the first case the  $\hat{n}$ -axis tilts away from the vertical *and back* so quickly compared to the precession of the spin that the spin hardly sees any change of the  $\hat{n}$ -axis in one revolution. In the second case the  $\hat{n}$ -axis moves so slowly that at any intermediate time the spin will precess around it many times before the tilt of the  $\hat{n}$ -axis has significantly changed. Hence the small changes will almost average away and the projection  $\hat{S} \cdot \hat{n}$  will hardly change. In all other cases polarization will be lost to some extent! This behaviour has been observed in many *low energy* accelerators and therefore the model is quite popular and well understood. Unfortunately at high energy, resonance strengths are increased due to the higher fields needed to focus the beam, and as  $\epsilon$  becomes larger the region in  $\nu_0 - Q$  over which the resonance strongly influences the spin motion becomes larger too. The single resonance model is based on the assumptions that the resonances are isolated. At high energy this is no longer true. Also the single resonance model cannot handle higher order resonances that have to be taken into account at high energy.

## 2.4 Siberian Snakes

A Siberian Snake, often also called full snake or 180° snake, is a magnetic device that

- rotates the spin by  $\pi$  around a particular axis called the snake axis and *ideally* does this independent of reference energy and phase space position,
- is optically transparent (almost).

There are two different families of snakes

- Solenoidal snakes:

A solenoid can be used to form a snake via the longitudinal term in (4). The snake axis of such a snake is always longitudinal. Unfortunately the spin rotation is energy dependent and the solenoidal snake therefore has to be ramped in order to supply a constant  $\pi$  rotation. The transverse coupling introduced by the solenoid has to be compensated by a suitable arrangement of skew quadrupoles. For technical reasons solenoidal snakes, even with superconducting technology, are almost impossible for energies of more than 3 GeV.

- Dipole snakes:

For big value of  $\gamma$  the transverse term in (4) is independent of energy. At sufficiently high energy an integrated field of 2.74 Tm always rotates the spin by  $\frac{\pi}{2}$ . Therefore we can make a closed combined vertical and horizontal bump that, due to non-commutation of rotations, rotates the spin by  $\pi$  around some axis. The direction of this snake axis can be chosen almost arbitrarily at the design stage. There are proposals [17] for snakes with tunable snake axis in operation without changing the spin rotation angle. Dipole snakes can be operated with fixed current. Snakes with discrete horizontal and vertical or even  $45^\circ$  tilted dipoles are possible as well as snakes with helical dipoles. Usually superconducting magnets are needed to obtain the necessary large integrated fields. Unfortunately at low energy the typical integrated fields produce an unbearably large orbit bump so that dipole snakes cannot be used much below 10 GeV.

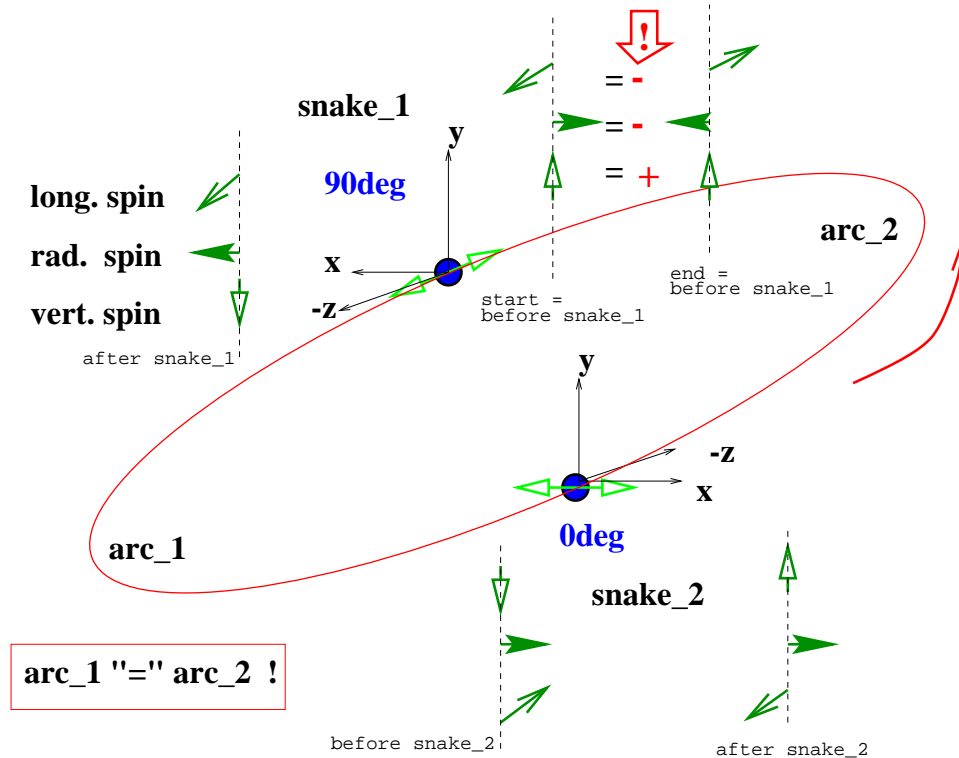


Figure 5: The effect of a longitudinal and a radial snake on spin motion on the design orbit: An orthonormal spin basis is tracked once around the machine. The vertical spin is mapped to itself whereas the radial and longitudinal spins are reversed. Hence:  $\hat{n}_0 = \hat{u}_y$  and  $\nu_0 = \frac{1}{2}$ .

There is also the “little brother” of the Siberian Snake — the partial snake. A partial snake introduces an energy dependent spin perturbation so large that total spin flip on crossing of imperfection resonances is guaranteed. Since it cannot overcome the depolarizing effects of intrinsic resonances, we will not go any deeper into its functionality nor the way to build it.

Inserting properly chosen Siberian Snakes into an accelerator has two main effects on spin dynamics

- The design orbit spin tune  $\nu_0$  can be fixed to  $\frac{1}{2}$  independently of energy.
- The  $\hat{n}$ -axis on the design orbit  $\hat{n}_0$  can be fixed into a certain direction independently of energy.

If we for example take a flat ring with an even number  $N_s$  of snakes with all their snake axes in the horizontal plane, then introducing the “Steffen angle”  $\beta$  which is twice the angle between the snake axis and the radial axis, it can be strictly proven that

1. The vertical axis ( $\hat{u}_y$ ) is an  $\hat{n}_0$ -axis.
2. The design orbit spin tune is

$$\nu_0 = \frac{1}{2\pi} \sum_{j=1}^{N_s} (-1)^j (\beta_j + \psi_j(E)) \quad , \quad (35)$$

where  $\psi_j = G\gamma \sum \phi_{\text{bends}}$  is the accumulated precession angle around the vertical direction of the arc section between snake  $j$  and  $j + 1$ .

3. If  $\nu_0$  is not an integer then  $\hat{n}_0 = \hat{u}_y$  is unique up to its sign all along the ring.

Here the  $\psi_j$  are the energy dependent spin rotations on the design orbit due to the arc sections between snakes, i.e.  $G\gamma$  times the total horizontal deflection angle of this section. We conclude that if snakes are placed in such a way that  $\sum_{j=1}^{N_s} (-1)^j \psi_j(E)$  vanishes, the contributions of the arcs cancel globally and the spin tune is independent of energy. The best choice of course is to make two adjacent sections compensate each other:  $\psi_{2j+1} = \psi_{2j}$ , so that the spin perturbations are hopefully cancelled as locally as possible.

Figure 5 shows how a scheme with a radial and a longitudinal snake placed in between two identical arc sections works to fix the spin tune at  $\nu_0 = \frac{1}{2}$  and make the  $\hat{n}_0$ -axis vertical independently of energy.

Spin motion on synchro-betatron-trajectories unfortunately is not that simple. Even with carefully chosen snake schemes there is an amplitude dependent spin tune spread over the particles of the beam. Each torus has a spin tune shifted by some  $\delta\nu(\vec{J})$

$$\nu_s(\vec{J}) = \nu_0 + \delta\nu(\vec{J}) \quad ; \quad \delta\nu(\vec{0}) = 0 \quad . \quad (36)$$

Furthermore the  $\hat{n}$ -axis will not be vertical all over phase space, although with linear  $\vec{\Omega}(\vec{z})$  for a flat machine without closed orbit distortion the averaged  $\hat{n}$ -axis  $\hat{u}_{(\hat{n})}(\vec{J}, l)$  is parallel to  $\hat{n}_0(l)$ . In the case of HERA-p which has vertical bends this is no longer true at most energies and azimuthal positions. Figure (6) shows the static polarization limit  $P_{\text{lim}}(\vec{J})$  in the energy range from 814 to 820 GeV for the flat model of HERA-p with vertical bends switched off (top) and for the '96 luminosity optics with 4 snakes (bottom). Additionally the vertical bend sections

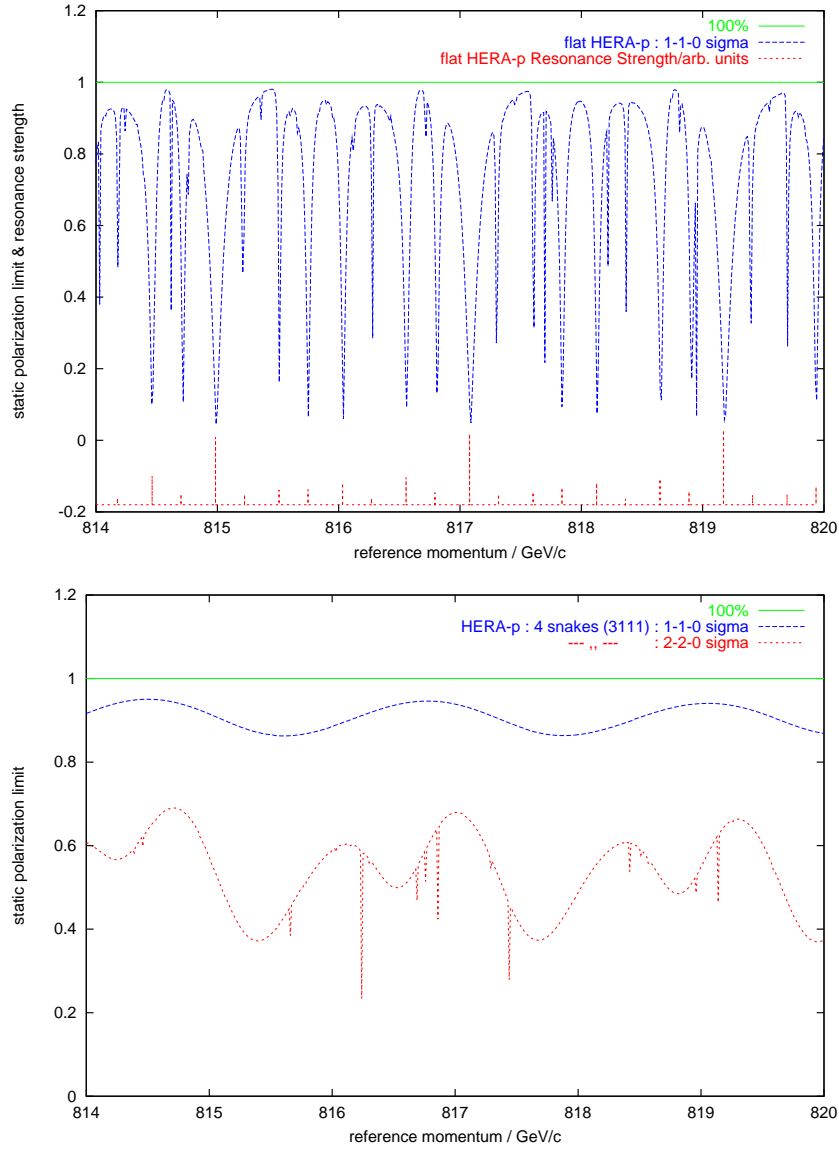


Figure 6: The static polarization limit  $P_{\text{lim}}$  for the 96' luminosity optics: (top): No snakes were installed and the lattice was made flat by switching off the vertical bending magnets. The first order resonance strengths for pure vertical motion are also plotted. (bottom): 4 snakes were installed and the vertical bends switched on but partially compensated by six “flattening snakes”.

were partially compensated by special extra snakes. For the flat HERA  $P_{\text{lim}}$  is computed on the invariant torus given by  $(\varepsilon_x = 4, \varepsilon_y = 4, \varepsilon_z = 0) \times \pi$  mm mrad or in beam widths as  $1\sigma-1\sigma-0\sigma$ . The relative resonance strengths in arbitrary units are plotted below  $P_{\text{lim}}$ . The polarization drops to zero at the exact positions of resonances as proposed in section 2.3. The bottom picture shows  $P_{\text{lim}}$  for HERA-p with a certain snake configuration on the invariant tori corresponding to the beam widths  $1\sigma-1\sigma-0\sigma$  and  $2\sigma-2\sigma-0\sigma$ . Obviously the energy dependence of  $P_{\text{lim}}$  is smoothed out if snakes are introduced. Also there is a periodic structure in the polarization curve that reflects the periodicity of the resonance structure but is shifted by some  $\delta\nu(\vec{J})$ . With properly chosen snakes the design orbit spin tune is  $\frac{1}{2}$ . This shows that snakes cannot totally compensate accumulation of spin perturbations on betatron trajectories nor will they fix the amplitude dependent spin tune  $\nu_s(\vec{J})$  in the same way that they fix  $\nu_0$ .

Whenever snakes are placed inside a lattice the approximate symmetry of the lattice has to be taken into account. At least the accumulated horizontal bend angle of the sections between snakes has to be adjusted to make (35) energy independent. Since HERA-p has approximate 4-fold symmetry, only schemes with  $2^n$  snakes seem adequate. Any snake arrangement taken into account for further studies should at least satisfy the following constraints

1. the spin tune on the design orbit is  $\nu_0 = \frac{1}{2}$
2. the  $\hat{n}_0$ -axis is vertical in the arcs.
3. the snake positions must be technically feasible and reflect the approximate four-fold symmetry of the HERA-p lattice.

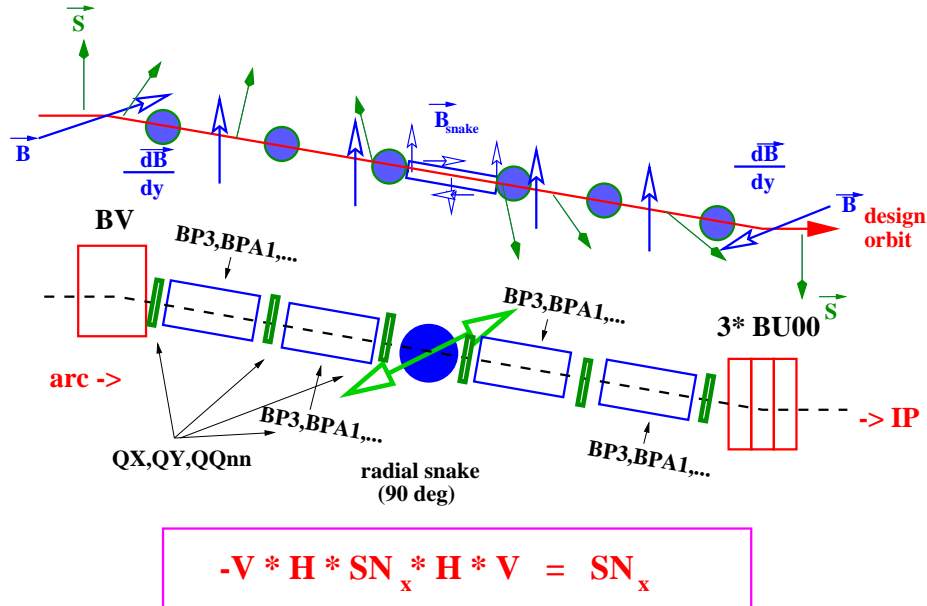


Figure 7: The design orbit spin perturbation of the vertical bends sections around the North-, South- and East-IP is effectively cancelled by inserting radial full snakes in the symmetry points of these sections

Equation (35) is only valid for a flat ring. HERA-p has vertical bend sections around the North-, East- and South-IP. The beam coming from the arc is bent downwards by 5.74 mrad ( $\equiv \phi_v$ ) then bent horizontally towards the centre by 4 times 15.10 mrad ( $\equiv \frac{1}{2}\phi_h$ ) and finally it is bent upwards by 5.74 mrad ( $\equiv -\phi_v$ ). In between there are some quadrupoles, but as long as the



design orbit is considered they do not affect the spin motion. The reverse procedure is applied after the IP. The spin precession on the design orbit of these sections is energy dependent and can be represented by the concatenated spin maps  $\underline{R}_{\hat{x}}(-G\gamma\phi_v)\underline{R}_{\hat{y}}(G\gamma\phi_h)\underline{R}_{\hat{y}}(G\gamma\phi_h)\underline{R}_{\hat{x}}(G\gamma\phi_v)$  and  $\underline{R}_{\hat{x}}(G\gamma\phi_v)\underline{R}_{\hat{y}}(G\gamma\phi_h)\underline{R}_{\hat{y}}(G\gamma\phi_h)\underline{R}_{\hat{x}}(-G\gamma\phi_v)$  respectively. It can easily be shown [5],[18] that inserting a radial “flattening” snake  $\underline{R}_{\hat{x}}(\pi)$  right in the symmetry point of a vertical bend section makes it act like a radial snake at the entrance of the straight section

$$\underline{R}_{\hat{x}}(\pm G\gamma\phi_v)\underline{R}_{\hat{y}}(G\gamma\phi_h)\underline{R}_{\hat{x}}(\pi)\underline{R}_{\hat{y}}(G\gamma\phi_h)\underline{R}_{\hat{x}}(\mp G\gamma\phi_v) = \underline{R}_{\hat{x}}(\pi) \quad , \quad (37)$$

taking into account only spin motion on the design orbit. Note that the two flattening snakes at the beginning and the end of the straight sections cancel each others spin rotations on the closed orbit  $\underline{R}_{\hat{x}}(\pi)\underline{R}_{\hat{x}}(\pi) = \underline{I}$  and that 60.4 mrad ( $= 2\phi_h$ ) horizontal bend angle have to be subtracted from the spin precession balance per vertical bend section if the flattening snakes are active. Of course the accumulated horizontal bend angles of the straight sections in between the vertical bend sections have to be fixed to 0 in order to fulfill the symmetry constraints for making (35) energy independent. Figure 7 shows schematically how the “flattening” method works for one of the six vertical bend sections. In the following we will only consider snake schemes with 6 radial, “flattening” snakes and  $2^n$  snakes chosen to optimize polarization. We will restrict ourselves mainly to  $n = 2$  and therefore a total of  $N_s = 10$  snakes, but will also show some examples with  $n = 3$  and thus  $N_s = 14$  snakes. We further assume that the “flattening” snakes have radial snake axes. Therefore we will speak of “4–snake–schemes” in the case of  $n = 2$  where the snakes are placed in the straight sections close to the IPs, and of “8–snake–schemes” in the case of  $n = 3$  where we additionally have 4 snakes in the centres of the arcs.

Even with the above restrictions there is a large number of possible snake schemes but only a small fraction will have good  $\hat{n}$ -axis behaviour over a reasonable energy range. The large number can neither all be checked by hand nor with time consuming non-perturbative techniques [9]. Thus for a first scan through the possible options a filtering algorithm [12],[6] is used. After fixing the snake *positions* and some set of energies, filtering consists of two principle steps

1. Test whether the constraints  $\hat{n}_0 = \hat{u}_y$  in the arcs and  $\nu_0 = \frac{1}{2}$  are fulfilled.
2. For the schemes that survived step 1 use a fast *linear* method for computing the polarization at the chosen energies. The linear method is only valid for moderate orbital amplitudes.

The schemes are then sorted by linear polarization and written to a file. In section 4 we will show some recent results of tracking analysis for some snake schemes.

## 2.5 The Acceleration Process

Up to this stage with the exception of the Froissart Stora formula (34) we only considered spin motion at constant energy  $E_0$ . Since there is no mechanism to polarize protons at high energy that looks half way promising, we have to accelerate polarized protons almost from rest to the desired working energy of HERA-p. At 820 GeV  $G\gamma$  is about 1570. Note that for  $G\gamma = 1570$  an orbital deflection of 1 mrad causes a spin precession of  $90^\circ$  ! Hence there are about 1570 imperfection resonances and  $2 \times 1570$  first order vertical resonances to cross. Equation (28) setting  $PM = 4 \times 26$  implies that just about 32 of them are particularly dangerous. However at a spin enhancement factor of more than 1500 even the weaker vertical resonances plus the

horizontal resonances plus the synchrotron sidebands plus the higher order resonances are wide enough to collectively perturb polarization in a severe way.

For constant reference energy the spin action  $J_s \equiv \hat{S} \cdot \hat{n}$  is an invariant of motion. Every spin rotates around its local  $\hat{n}$ -axis. Hence  $P_{\text{dyn}}(\vec{J})$  is a constant for all  $\vec{J}$  too.

In the case of changing  $\gamma_0 = \frac{E_0}{m}$  the spin action  $J_s$  can be shown to be an adiabatic invariant [13]. That means that as long as  $\gamma_0$  changes “slowly enough” with respect to some time scale,  $J_s$  will hardly change at all. At the first glance this seems trivial since the  $\hat{n}$ -axis is considered the “periodic solution” of the T-BMT equation and the angle between two solutions is conserved, but actually it’s not quite that simple. The T-BMT equation (5) determines the spin motion as an initial value problem (IVP) for a given trajectory  $\vec{z}(l)$  and arbitrary  $\vec{\Omega}$ . If we introduce an  $l$ -dependent  $\gamma_0$ ,  $\gamma_0(l)$ , the IVP for the spin reads

$$\begin{aligned} \frac{d\hat{S}_{\gamma_0}(\vec{z}_{\gamma_0}(l))}{dl} &= \vec{\Omega}(\vec{z}(l), l; \gamma_0(l)) \times \hat{S}_{\gamma_0}(\vec{z}_{\gamma_0}(l)) , \\ \hat{S}_{\gamma_0}(\vec{z}(l_0)) &= (\hat{S}_{\gamma_0})_0 , \end{aligned} \quad (38)$$

whereas the invariant spin field is determined by a periodic boundary problem with constant internal parameters

$$\begin{aligned} \frac{\partial \hat{n}_{\gamma_0}(\vec{z}(l), l)}{\partial l} + \frac{\partial \hat{n}_{\gamma_0}(\vec{z}(l), l)}{\partial \vec{z}} \cdot \frac{d\vec{z}}{dl} &= \vec{\Omega}_{\gamma_0}(\vec{z}(l), l) \times \hat{n}_{\gamma_0}(\vec{z}(l), l) , \\ \hat{n}_{\gamma_0}(\vec{z}, l + L) &= \hat{n}_{\gamma_0}(\vec{z}, l + L) , \\ \gamma_0 &= \text{const.} . \end{aligned} \quad (39)$$

Therefore each  $\gamma_0(l)$  leads to a potentially totally different  $\hat{n}$ -axis! In figure 6 of section 2.4 we could already observe such an effect. The  $\hat{n}$ -axis on some torus was computed for different energies independently. Not only does  $\hat{n}_{\gamma_{0,1}}(\vec{z}, l)$  differ from  $\hat{n}_{\gamma_{0,2}}(\vec{z}, l)$  for different  $\gamma_{0,1}, \gamma_{0,2}$  but even the angle averaged polar opening angle on the torus  $\alpha(\vec{J})$  and hence the static polarization limit  $P_{\text{lim}}(\vec{J})$  are more or less strongly dependent on energy.

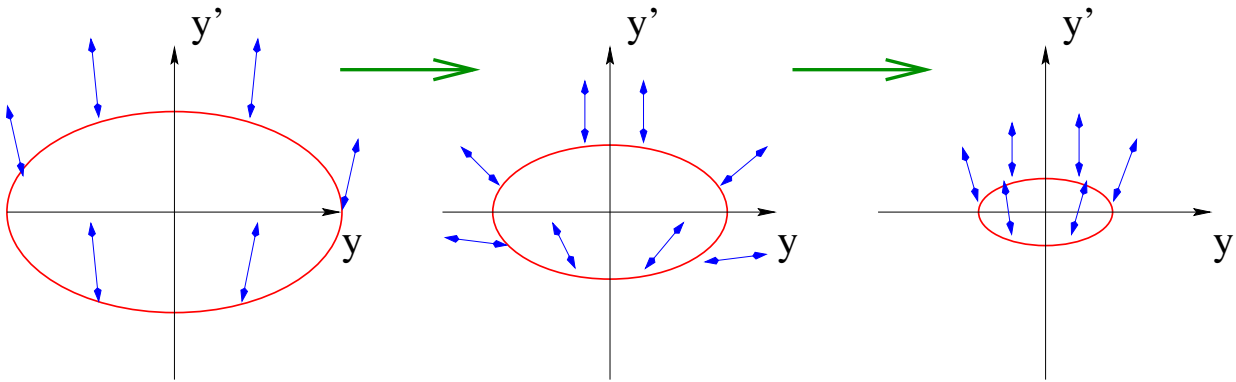


Figure 8: The opening and closing of the  $\hat{n}$ -distribution at ramp time. As the energy is increased (from left to right), the angular spread of the  $\hat{n}$ -distribution will increase in energy ranges of strong spin perturbations but will decrease again after exiting these regions. A suitable working point is clearly at an energy where the average opening angle is small so that the static polarization limit is high.

By definition the  $\hat{n}$ -axis distribution does not depend on the acceleration process. In certain energy regions the opening angle will be large but we can always find a region where it becomes

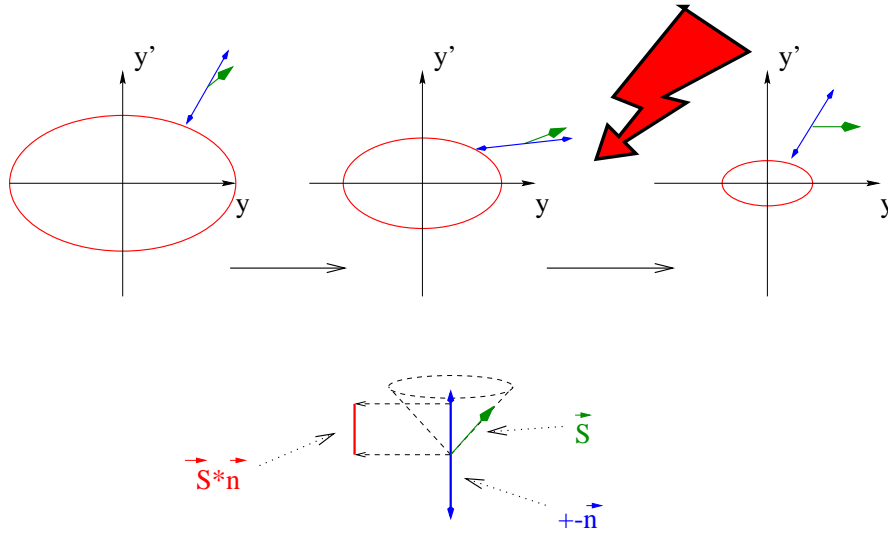


Figure 9: Polarization loss due to non-adiabatic spin motion at ramp time. As long as the spin motion is adiabatic the projection  $\hat{S} \cdot \hat{n}$  will almost stay constant. At certain energies the  $\hat{n}$ -axis might change so quickly that the spin cannot follow completely. Hence  $\hat{S} \cdot \hat{n}$  will change.

moderate again, to some extent even without snakes. The invariant spin field is related to the lattice and the *current* energy only — it does *not* depend on history! Figure 8 illustrates this property of the  $\hat{n}$ -axis. But  $J_s$  and therefore the dynamic polarization  $P_{\text{dyn}}$  can suffer. As long as  $\hat{n}(\vec{z}_{\gamma_0}(l), l; \gamma_0(l))$  is well defined for all  $l$  we obtain for the change of  $J_s = \hat{S} \cdot \hat{n}$  during the history of acceleration,

$$\frac{d}{dl} \left[ \hat{S}_{\gamma_0}(\vec{z}_{\gamma_0}(l)) \cdot \hat{n}(\vec{z}_{\gamma_0}(l), l; \gamma_0(l)) \right] = \hat{S}_{\gamma_0}(\vec{z}_{\gamma_0}(l)) \cdot \frac{\partial \hat{n}(\vec{z}_{\gamma_0}(l), l; \gamma_0(l))}{\partial \gamma_0} \frac{d\gamma_0(l)}{dl}. \quad (40)$$

Now we are able to discuss the content of (34) qualitatively. Locally,  $\hat{S}$  rotates around the  $\hat{n}$ -axis. Since  $\hat{n}$  is a unit vector,  $\frac{\partial \hat{n}}{\partial \gamma_0}$  has to be perpendicular to  $\hat{n}$ . Hence only  $\vec{S}_{\perp} = \hat{S} - J_s \hat{n}$  contributes to (40). If  $\hat{S}$  and therefore  $\vec{S}_{\perp}$  rotates so quickly compared to the rate of change of the  $\hat{n}$ -axis that small changes in  $\hat{n}$  are almost averaged away in each turn,  $J_s$  is therefore almost constant. In other words the spin can follow the changing  $\hat{n}$ -axis almost completely. If on the contrary  $\frac{\partial \hat{n}}{\partial \gamma_0}$  is zero most of the time except for a very short interval where the  $\hat{n}$ -axis turns by  $180^\circ$  before the spin can follow, then in the integral  $\Delta J_s = \int_{\gamma_1}^{\gamma_2} \hat{S} \cdot \frac{\partial \hat{n}}{\partial \gamma_0} d\gamma_0$ , the spin can be taken as constant and  $J_s$  almost reverses its sign. In all other cases  $|J_s|$  will change and therefore  $P_{\text{dyn}}$  usually will drop.  $\frac{\partial \hat{n}}{\partial \gamma_0}$  is particularly big in energy regions with strong resonances. Note that in the Froissart Stora formulation the polarization is measured with respect to a fixed unit vector namely  $\hat{u}_y$  whereas in the invariant spin field formulation the polarization is measured with respect to  $\hat{n}$ . The propagated  $\hat{n}$ -axis i.e.  $\hat{n}(\vec{z}_{\gamma_0}(l), l; \gamma_0(l))$  evaluated along an orbital trajectory changes its sign at resonance crossing. Hence  $\frac{J_{s,2}}{J_{s,1}} \approx 1, -1$  in the invariant spin field formulation corresponds to  $\frac{P_{\text{dyn}}(l=+\infty)}{P_{\text{dyn}}(l=-\infty)} \approx -1, 1$  in the Froissart Stora formulation. Figure 9 illustrates the potential loss of  $J_s$  for a chosen particle when crossing a resonant region. The above calculations are based on the assumption that  $\hat{n}(\vec{z}_{\gamma_0}(l), l; \gamma_0(l))$  is well behaved. After crossing an energy region  $[\gamma_1, \gamma_2]$  where the  $\hat{n}$ -axis along the particle trajectory  $\hat{n}(\vec{z}_{\gamma_0}(l), l; \gamma_0(l))$  is ill-defined i.e. undefined or multi-valued the difference in  $\Delta J_s$  can be arbitrary as long as  $J_s \in [-1, 1]$  is fulfilled.

There is another source of depolarization related to the dependence of the spin motion on the phase space torus. Since the  $\hat{n}$ -axis is defined by a periodic boundary problem rather than by an initial value problem, the  $\hat{n}$ -axis for fixed  $\gamma_0$  is only unique up to its sign. Usually by convention the vertical component of  $\hat{n}$  is fixed to point upwards, but under static conditions ( $\vec{z}, l : \text{const.}$ )  $\hat{n}(\vec{z}, l)$  is fully equivalent to  $-\hat{n}(\vec{z}, l)$ . So when computing  $\hat{n}(\vec{z}(l_0), l_0)$  for one point in phase space we have the freedom to choose its sign. If we require  $\hat{n}$  to be smooth, then by using (10) the signs of  $\hat{n}$  at all other points ( $\vec{z}(l), l$ ) on the trajectory starting at  $(\vec{z}(l_0), l_0)$  are already fixed. If all tunes are incommensurable, for  $l \rightarrow \infty$  the torus will be filled densely with unit vectors continuously connected to  $\hat{n}(\vec{z}(l_0), l_0)$  on the trajectory  $\vec{z}(l; \vec{z}(l_0))$ . Hence only the *initial* sign is actually free and the distribution  $\hat{n}_{\vec{J}, l} : [0, 2\pi]^3 \rightarrow \mathbb{S}_3, \vec{\Psi} \rightarrow \hat{n}(\vec{J} = \text{const}, \vec{\Psi}, l = \text{const})$  can fill the whole sphere. Now imagine an ensemble of  $N$  particles with spin  $(\hat{S}_{\gamma_0}^{(\hat{n})}(\vec{J}, \vec{\Psi}_i))_{1 \leq i \leq N}$  on the torus  $\vec{J} = \text{const.}$  with all spins upward parallel to their  $\hat{n}$ -axis ( $J_{s,i} = 1 \forall i$ ) initially. The distribution might be tightly bundled around the vertical upward axis, which implies  $\alpha \ll 1$ ,  $P_{\text{lim}} \approx 1$ , and  $\hat{u}_{\langle n \rangle} \approx \hat{u}_y$ . It is ramped through an energy region where we can neglect all non-adiabatic changes in the  $J_{s,i}$ , but the distribution  $\hat{n}_{\vec{J}, l}(\vec{\Psi})$  fills the whole unit sphere  $\mathbb{S}_3$ . We look at it at an energy where the distribution is tightly bundled again. There are two possibilities

1. The spin ensemble spread out all over the unit sphere while crossing the region of  $\alpha = \frac{\pi}{2}$  but comes back to the vertical upward direction afterwards.
2. The spin ensemble opens and in the end closes back to the vertical downward direction.

Case 1 is trivial but in case 2 the ensemble average has reversed its projection on the static polarization axis  $\hat{u}_{\langle n \rangle}$ , defined for constant energy. Therefore  $J_{s,i} = -1$  with respect to the static polarization axis and the ensemble average  $P_{\text{dyn}}$  has become  $-1$  too. As long as only *one* torus is considered this “spin flip” does not do any harm, but the total polarization contains contribution from all tori (22). Some might have “flipped” some might not. Hence the contributions from “flipped” and “non-flipped” tori have to be subtracted. Of course this can happen only after crossing a region with  $\alpha_{\gamma_0}(\vec{J}) = \frac{\pi}{2}$ . In principle this “spin flip” is reversible since it is an adiabatic process, but most likely the number of tori with different orientations of  $\hat{u}_{\langle n \rangle}$  (up or down) will increase rather than decrease after each energy range with  $\alpha_{\gamma_0}(\vec{J}) = \frac{\pi}{2}$ . Mainly because the  $\vec{J}$  where branching occurs depends on the resonance structure which is not likely to be repeated exactly since resonances tend to get stronger with increasing energy. Therefore an additional serious topic in preserving polarization is minimizing the number of energies with  $\exists \vec{J} \in [0, J_{\text{max}}]^3 : \alpha_{\gamma_0}(\vec{J}) \approx \frac{\pi}{2}$ .

### 3 The HERA-p pre-accelerator chain

Polarized protons have to be produced in the source. Then on accelerating up to the working energy the polarization should be preserved as much as possible. There seems to be no way of recovering from depolarization at high energy. Furthermore the experiments demand that the luminosity for polarized runs should not less than for unpolarized runs.

### 3.1 The $H^-$ source

Currently DESY only has an unpolarized magnetron source that is able to produce about 60 mA of  $H^-$ -ions. A pulsed optically pumped polarized ion source (OPPIS) is under construction at TRIUMF [14]. The goal for the operational parameters is

$H^-$ current	$\geq 20$ mA
polarization	$\geq 80$ %
emittance (transv.)	$\leq 2\pi$ mm mrad
pulse duration	100 $\mu$ s
repetition rate	.25 Hz

With this or a similar source and an optimized match to the RFQ and LINAC-III the injection current into DESY-III, which is roughly 10–20 mA in 10 bunches at the moment, could almost be conserved. With the '98 run period the DESY  $H^-$  injection will have a switch-able MEFT connecting two LEBTs and RFQs with LINAC-III. So changing from polarized to unpolarized operation could be done without long down-times. The polarization direction produced by the OPPIS is longitudinal, hence mounting the polarized source on the straight arm of the switch-yard is preferable from this point of view.

### 3.2 RFQ, LEBT, LINAC-III and transfer lines

Spin dynamics in the straight parts of the pre-accelerator chain is considered almost harmless for the following reasons:

1. The spin enhancement factor  $G\gamma$  is small.
2. At these energies the directional distribution of the invariant spin field at the entrance/exit of the following/preceding circular accelerator will be tightly bundled i.e.  $\alpha \ll 1$  since the transfer energy can be chosen to be off-resonance.
3. The strongest spin perturbations in circular accelerators arise from adding up small perturbations turn by turn. This is excluded for linear structures by definition.
4. The transfer lines and the LEBT don't change the particle's reference energy. They can be spin matched for exactly one energy.

Whether point number 1 still holds for the transfer line PETRA to HERA-p (PR-Weg) has to be analyzed separately. But anyway there are still some things to care about

1. In order to preserve luminosity the transfer efficiency has to be optimized.
2. The transfer lines from LINAC-III to DESY-III (HEBT), from DESY-III to PETRA (P-Weg), and PR-Weg include horizontal, vertical, and otherwise tilted bends. Hence they will apply an energy dependent rotation to the polarization. Since the projection  $\hat{S} \cdot \hat{n}$  is constant in periodic structures and for constant energy, the spin transfer function must be matched from the preceding to the following accelerator to maintain polarization. Note also that the polarization from the source is longitudinal, but in the circular machines it is preferably vertical.

Spin direction tuners are needed to tune the polarization axis and compensate the effect of interleaved horizontal and vertical bends. Spin direction tuners are snake-like devices operated at a single energy. This implies for the following different stages

- LEBT, RFQ, and LINAC-III: We must check whether some spin match for longitudinal polarization is necessary at all. Improving on transfer efficiency would help to maintain luminosity.
- HEBT: Most likely the best place to rotate polarization vector into vertical direction.
- P-Weg and PR-Weg: The polarization axis must be tuned to overcome the rotation from the tilted and vertical bends.

### 3.3 DESY-III

DESY-III is a strong focusing flat synchrotron with a super period of 8. Each period consists of 3 cells with 2 focusing and defocusing combined function magnets (BD, BF). Additionally each period has 4 independent quadrupoles (QD1, QF1, QD2, QF2). Multi-turn injection is done through a stripping foil. In standard operation 10 out of 11 RF-buckets are filled. Since the injection is at 50 MeV kinetic energy and ejection energy is 7.5 GeV, there are 14 imperfection resonances in the DESY-III energy range. DESY-III has 4 weak intrinsic resonances with strength .002—.01 corresponding to  $4\pi$  mm mrad vertical emittance [16]. The resonances are well separated so that the single resonance model seems applicable. The imperfection resonances can probably be overcome with a partial snake [14]. In order to overcome the intrinsic resonances either the method of tune jump can be applied [14], or resonance excitation with a vertical RF-dipole [15] can be used to ensure full spin flip at resonance crossing. To decide which of these methods seems more promising, a more detailed analysis is necessary. The large space charge tune spread at injection as well as the observed emittance blow up on the ramp have to be taken into account, both for spin as well as orbital stability.

### 3.4 PETRA-p

PETRA-p consists of 8 identical arcs with 13 FODO cells each. There are 4 long straight section (N, O, L, S) and 4 short straight sections (NO, SO, SW, NW). In standard operation 60 out of 400 RF-buckets are filled. Considering polarization it is unfortunate that the protons have to be bypassed around the electron RF in the South straight section. Hence the superperiodicity of PETRA-p is just 1. But there is mirror symmetry with respect to the North-South axis. There are many more intrinsic resonances in PETRA and they are up to 5 times stronger than in DESY-III. Therefore at the high energy part of the ramp they are close to overlapping [16]. In that region only Siberian Snakes are expected to preserve polarization. At the low energy end solenoidal snakes are already impossible and dipole snakes make large orbit distortion. It was proposed [14] to use two Siberian Snakes in PETRA. Problems arise from the length of warm snakes, estimated to be 13 m [14]. This has to be compared to the typical length of a drift space between quadrupoles of 7.5m. For superconducting snakes problems arise from the liquid helium which would be necessary.

### 3.5 Polarimeters

Clearly a high energy polarimeter suitable for 820 GeV is needed to supply the experiments with polarization data. But polarimeters are also needed at almost all stages of the pre-accelerator chain for diagnostics. Even if the LEBT–RFQ–LINAC section is spin transparent, polarimeters are needed at the following places and energies

- Source polarization: the polarization must be surveyed either directly after the source or somewhere before the HEBT implying an operating energy for the polarimeter somewhere in the region of a few keV to 50 MeV.
- The polarization must be measured after the HEBT or directly after injection into DESY–III in order to adjust the matching of the polarization direction. The required working energy is 50 MeV
- The polarization at DESY–III ejection must be measured to optimize orbit correction, snake and tune–jump or RF–dipole settings. At an energy of 7.5 GeV polarization measurements (e.g. with elastic  $p$ – $p$  scattering) already take a significant time. In order to adjust for compensating the intrinsic resonances step by step a procedure to eject the beam at energies other than 7.5 GeV is necessary.
- A polarimeter is needed at the end of the P–Weg or at injection into PETRA.
- It must be possible to measure polarization at different energies on the PETRA ramp from 7.5 to 40 GeV. If the P–Weg polarimeter is placed in PETRA, it could possibly handle the low energy end of this range. Note that PETRA cannot be cycled as quickly as DESY so that the time for a polarization measurement should be not much more than the beam lifetime in PETRA at the required energy.
- Since polarimetry at high energy takes longer and longer, there cannot be a polarimeter inside the PR–Weg and thus the spin transfer through the PR–Weg can only be controlled with the HERA “low energy” polarimeter.
- The spin perturbations are expected to be worst in HERA. Therefore at any stage of the ramp there must be an opportunity to measure the polarization. It is not clear yet how many polarimeters are needed to cover the whole energy range from 40 to 820 GeV. Most probably at least one more polarimeter is needed at the high energy end of the ramp.

A more detailed analysis on the pre-accelerator chain can be found in [14], but it has to be mentioned that a complete analysis including spin tracking with snakes in PETRA has not yet been carried out.

## 4 Conservation of Polarization when Ramping with Various Snake Schemes

In this section we will report on the latest results of simulations for the polarized protons project at HERA–p with the code `SPRINT` [6]. The static polarization limit in the energy region around 820 GeV was extensively studied [19]. Here we will concentrate on the polarization losses while ramping through the 803 GeV resonant region.

Various snake schemes based on a slightly modified 820 GeV separation optics from '96 (called `hp96se820y`) will be discussed. The slight modifications are equivalent to those applied to the '96 luminosity optics in [19]. They are introduced to make the ring close to a high degree of accuracy and to make the interaction regions exactly  $90^\circ$  apart from each other. The  $3 \times 2$  vertical bend sections around the North-, East- and South-IP where compensated (on the design orbit) with “flattening snakes”. The 4 main Siberian Snakes were placed in the octants NL, OR, SR directly after the superconducting vertical BV magnet as seen from the interaction point (IP) and in the straight section around the West IP. The snake positions are at places where drift spaces of about 10 m can be created without too much effort.

Four schemes with 4 snakes plus flatteners were tested and one scheme with 8 snakes. The 4 additional snakes are placed in the centres of the arcs, i.e. “on” the cryo supplies. The 8-snake scheme is mainly of theoretical interest, but there are proposals for “bending snakes” that could replace dipoles in the arcs [20]. The schemes are (see [19] for naming convention).

- ‘3111’ : A longitudinal snake in the East and radial snakes in the North, West and South straight sections.
- ‘1b1b’ : Radial snakes in the East and West straight sections and  $45^\circ$ -snakes in the North and South. Figure 10 gives a schematic view of ‘3111’ as well as ‘1b1b’.
- ‘3e1b’ : A longitudinal snake in the East a radial snake in the West and two  $\pm 45^\circ$ -snakes at the South and North IPs. This scheme minimized the linear opening angle averaged over the interval from 39.5 GeV to 821.5 GeV.
- ‘1d3c’ : A radial snake in the East, a longitudinal snake in the West and  $\pm 67.5^\circ$ -snakes at the South and North IPs. This scheme minimized the linear opening angle in the same energy range *but with the luminosity optics!* ‘3e1b’ and ‘1d3c’ are shown in figure 14.
- ‘33e111b3’ : Actually means ‘3e1b’ plus 2 radial and 2 longitudinal snakes in the centres of the arcs. It minimized (among the 8-snake schemes) the linear opening angle from 39.5 GeV to 821.5 GeV with the luminosity optics and was tested with the luminosity optics. The configuration is shown in figure 18.

The ramp simulation was made for all schemes in the following way:

1.  $l_0$  is at the East IP.
2. A particle with initial phase space coordinates  $\vec{z}_0 = \vec{z}(\vec{J}_\sigma, \vec{\Psi}_0)$  on a torus with all 3 normalized emittances equivalent to the same beam- $\sigma$  (namely 1, 1.5, 2 and 2.5) and azimuthal position  $l_0$  was chosen.
3. In the energy region from 785 to 788 GeV the  $\hat{n}$ -axis was scanned in order to find a good starting energy where the accuracy for the computation of the initial  $\hat{n}$ -axis is high. Let  $E_i$  be this optimal energy.
4. A spin  $\hat{S}_{\hat{n}}(\vec{z}_0, l_0; E_i)$  was set parallel to  $\hat{n}_{E_i}(\vec{z}_0, l_0)$ .
5. The spin was tracked some number of turns with constant energy. The average direction of the tracked spins at  $(\vec{J}_\sigma; E, l_0)$

$$\hat{u}_{(S)}(\vec{J}_\sigma; E, l_0) \equiv \frac{\left\langle \hat{S}_{\hat{n}}(\vec{z}(l_0 + kL), l_0 + kL; E_i) \right\rangle_k}{\left\| \left\langle \hat{S}_{\hat{n}}(\vec{z}(l_0 + kL), l_0 + kL; E_i) \right\rangle_k \right\|} \quad (41)$$



and the average projection of the tracked spins on this direction

$$P_{\langle S \rangle}(\vec{J}_\sigma; E, l_0) \equiv \langle \hat{S}_{\hat{n}}(\vec{z}(l_0 + kL), l_0 + kL; E) \cdot \hat{u}_{\langle S \rangle}(\vec{J}_\sigma; E, l_0) \rangle_k \quad (42)$$

was computed and plotted. Note that if the spin stays parallel to  $\hat{n}$  all over the ramp, these parameters are just  $\hat{u}_{\langle n \rangle}$  and  $P_{\text{lim}}$  respectively. We will refer to  $P_{\langle S \rangle}$  as the “one particle multi turn” polarization.

6. The one spin system was ramped over some energy range  $\Delta E_{\text{plot}} = .5 \text{ GeV}$ . The energy increase per turn was taken to be 13 keV which is the average energy increase on the HERA-p ramp.
7. Step 5 to 7 were repeated with  $\hat{S}_{\hat{n}}(\vec{z}_0, l_0; E_i)$  being replaced by  $\hat{S}_{\text{rmp}}(\vec{z}_{\text{rmp}}, l_0; E_{\text{rmp}})$  until 825 GeV were reached.


This simulates an energy ramp that starts somewhere in between 785 and 788 GeV with  $P_{\text{dyn}}(\vec{J}_\sigma; E_i, l_0) \equiv 1$ . In figures 11, 12, 13 15, 16, 17, 19 and 20 the “one particle multi turn” polarization  $P_{\langle S \rangle}(\vec{J}_\sigma; E)$  is plotted versus reference momentum for the above snake schemes and various invariant phase space tori. The plots also include the static polarization limit  $P_{\text{lim}}(\vec{J}_\sigma; E)$  and as a reference the resonance structure for flat HERA-p.

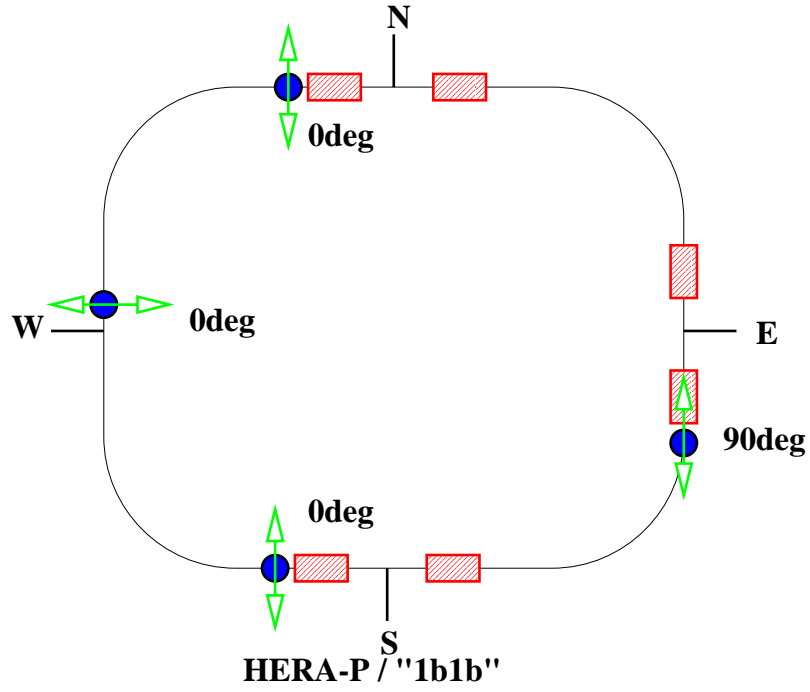
Figure 11 shows the ramp simulation for the ‘3111’ scheme on the  $1\sigma$ - $1\sigma$ - $1\sigma$  torus (top) and the  $1.5\sigma$ - $1.5\sigma$ - $1.5\sigma$  torus (bottom). The static polarization limit  $P_{\text{lim}}$  was computed with the non-perturbative stroboscopic averaging algorithm [9] and is therefore called “non-perturbative polarization” in the figures. The ramped “one particle multi turn” polarization stays close to the static polarization limit until the ramp hits the resonant area around 803 GeV. The ramped polarization drops by 5% in the  $1\sigma$  case and by 40% in case of the  $1.5\sigma$ - $1.5\sigma$ - $1.5\sigma$  torus. Note that this is the strongest resonance but that there are at least 31 resonances with comparable strength and comparable density of neighbouring resonances to cross before reaching the 803 GeV region! Note also that the existence of depolarizing effects at the energy of strong first order resonances in the presence of snakes can have two main reasons: First the amplitude dependent spin tune shift  $\delta\nu(\vec{J}, E)$  might suffice to fulfill the resonance condition

$$\frac{1}{2} + \delta\nu(\vec{J}, E) = k \pm Q_y \quad , \quad (43)$$

or second the snake scheme might itself enhance the strength of higher order resonances (“snake resonances”) close to the linear resonance. In figures 12 and 13 we see the ramp simulation for the ‘1b1b’ scheme on the  $1\sigma$ - $1\sigma$ - $1\sigma$  torus (fig. 12 top), the  $1.5\sigma$ - $1.5\sigma$ - $1.5\sigma$  torus (fig. 12 bottom) and the  $2\sigma$ - $2\sigma$ - $2\sigma$  torus (fig. 13). We see that this scheme, although it has a higher snake super period (2 instead of 1 for ‘3111’), fails already at  $1\sigma$ . The polarization drops to 30% after resonance crossing. In the  $1.5\sigma$  case one might believe that polarization recovers, but after a closer look at the tracking data it becomes obvious that this is an artifact of the single particle simulation. Actually at  $1.5\sigma$ - $1.5\sigma$ - $1.5\sigma$  a neighbouring resonance (at approximately 807 GeV) is enhanced so much that the spin is pushed back closer to the  $\hat{n}$ -axis of the static system. The average spin direction  $\hat{u}_{\langle S \rangle}(\vec{J}_\sigma; E)$  is reversed twice in the  $1\sigma$  and 3 times in the  $1.5\sigma$  case. In a real spin ensemble an additional spin kick would tend to destroy the angular coherence of the ensemble instead of kicking *all* spins back to their  $\hat{n}$ -axis. The worst case for the  $i$ -th particle occurs when  $\hat{S}_{\gamma_0, i}(\vec{z}(l_1), l_1)$  is perpendicular to  $\hat{n}(\vec{z}(l_1), l_1; \gamma_0(l_1))$  which is equivalent to  $|J_{s, i}(l_1)| \equiv 0$ . Then the next “depolarizing kick” at  $l_2 > l_1$  can only *increase* the

HERA-P / "3111"

 =  $-V * H * SN_x^* H * V$



 =  $-V * H * SN_x^* H * V$

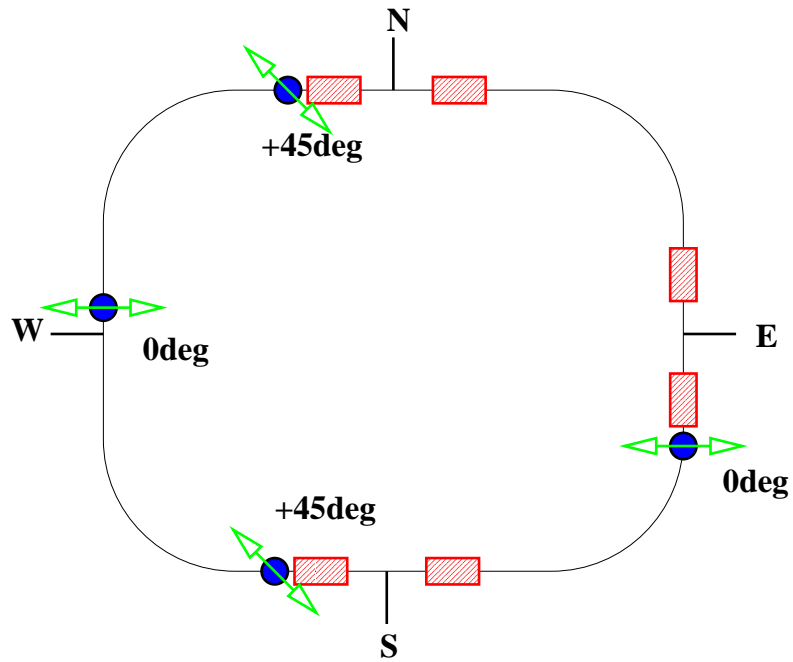


Figure 10: The snake schemes '3111' and '1b1b'

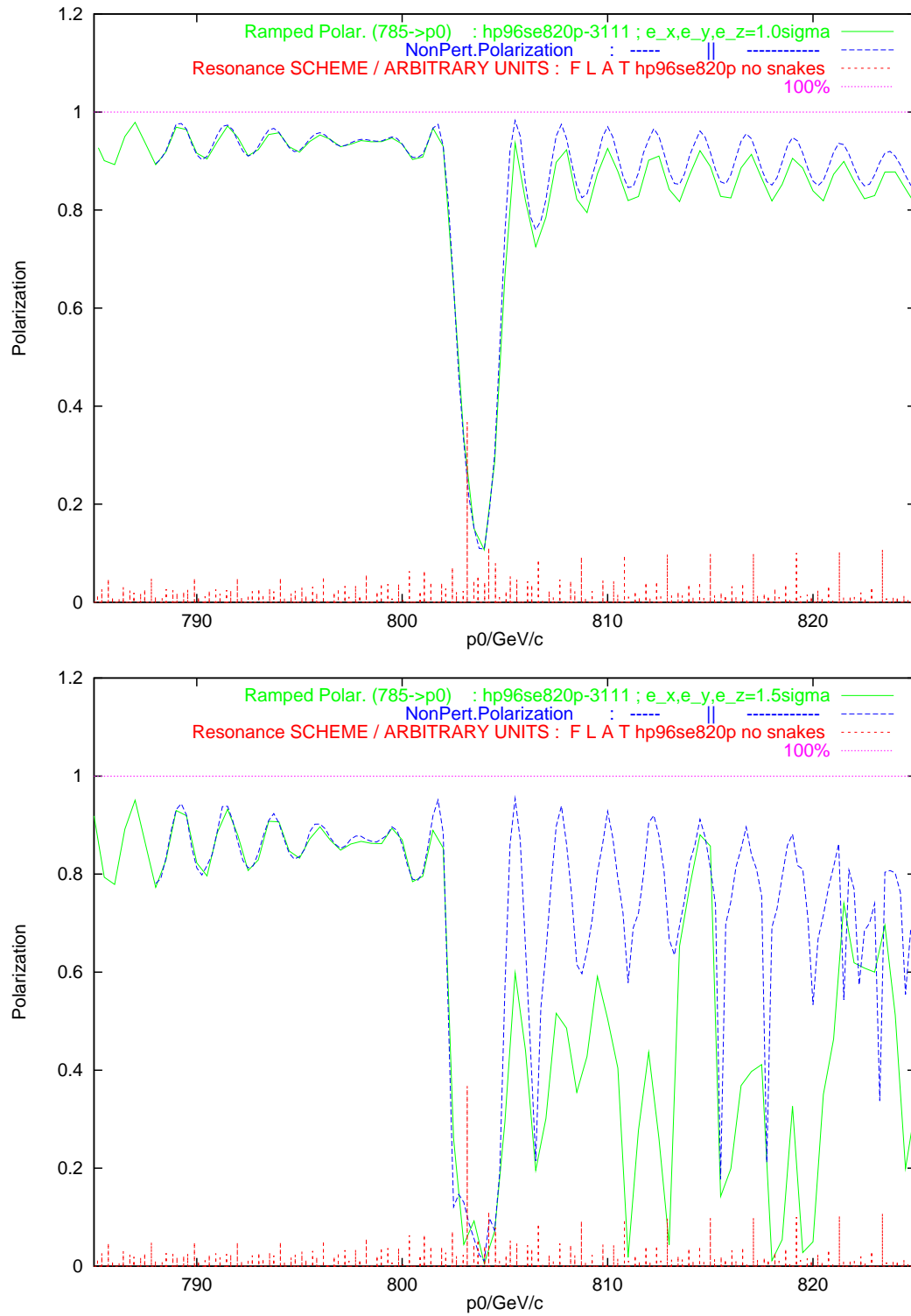


Figure 11: Scheme '3111': comparison between  $P_{(S)}$  and  $P_{lim}$  for 1.0 (top) and 1.5  $\sigma$  (bottom) in all 3 planes

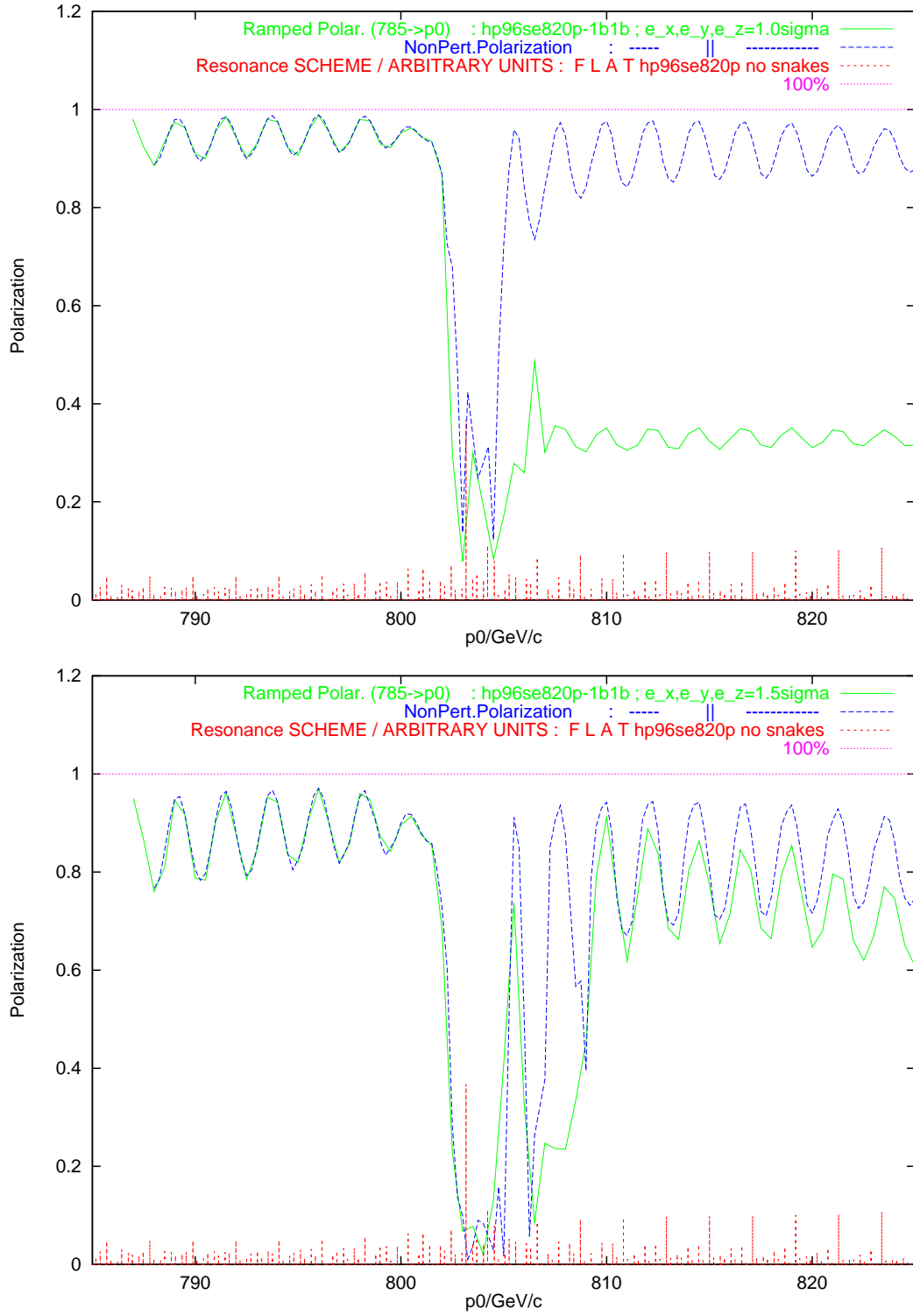


Figure 12: Scheme '1b1b': comparison between  $P_{(s)}$  and  $P_{lim}$  for 1.0 (top) and 1.5  $\sigma$  (bottom) in all 3 planes

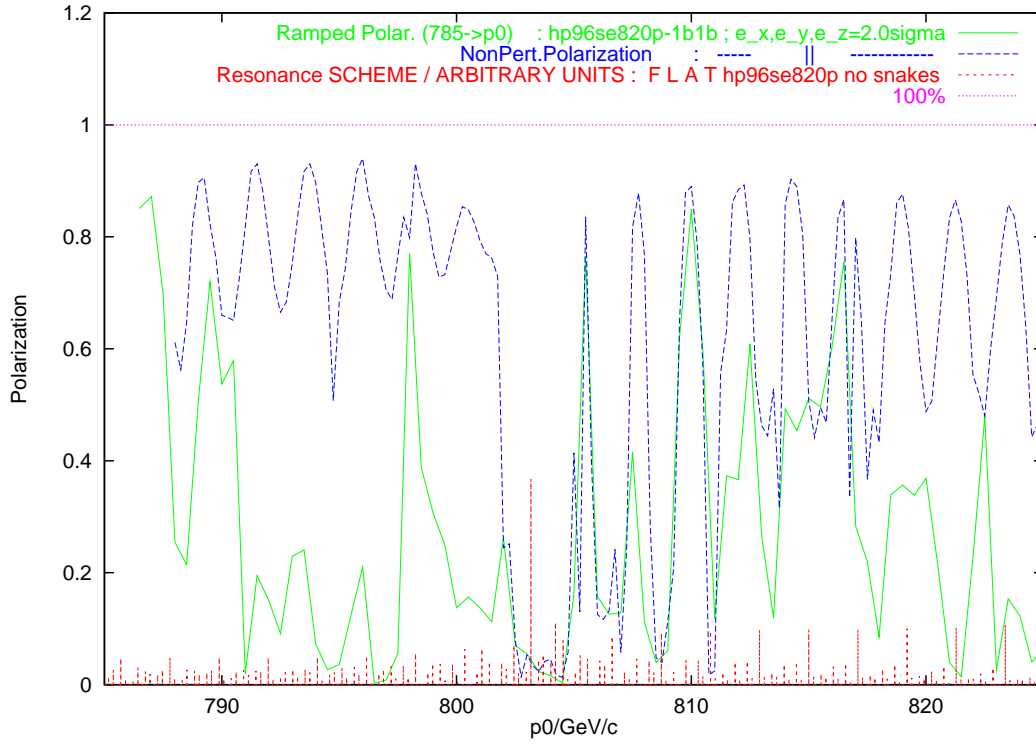


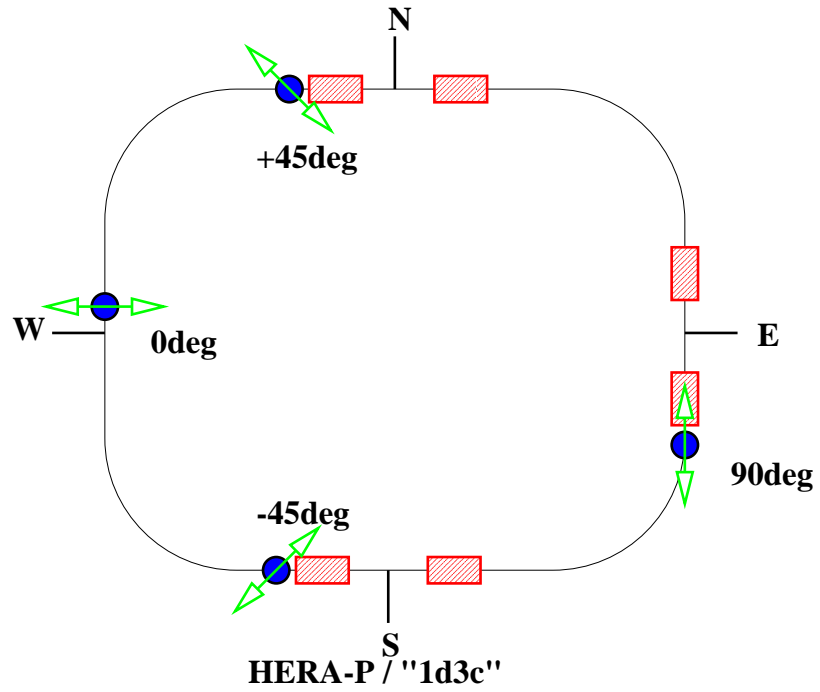
Figure 13: Scheme ‘1b1b’: comparison between  $P_{(S)}$  and  $P_{\text{lim}}$  for  $2.0\sigma$  in all 3 planes

absolute value of it’s projection on the  $\hat{n}$ -axis , hence  $|J_{s,i}(l_2)| \equiv J^+ > 0$  afterwards. But even if all spins  $1 \leq i \leq N$  at  $(\vec{z}, l)_{l_1 < l < l_2}$  receive a kick towards  $\pm \hat{n}$  of the same absolute strength, their projections  $(J_s)_i(l_2)$  will be almost symmetrically distributed in  $[-J^+, +J^+]$ . Therefore the ensemble average  $P_{\text{dyn}}(\vec{z}(l_2), l_2) \equiv \langle \hat{S}_{\gamma_0,i}(\vec{z}(l_2), l_2) \cdot \hat{n}(\vec{z}(l_2), l_2; \gamma_0(l_2)) \rangle_i$  will probably vanish. When dynamic polarization is lost it is lost for ever! At  $2\sigma$  the resonance width or the number of neighbouring snake resonances is enhanced so much that the polarization immediately decays on the ramp even far from the nominal resonance position.

Figures 15 and 16 show the result of the ramp simulation for the filtered ‘3e1b’ scheme. For the  $1\sigma$ - $1\sigma$ - $1\sigma$  torus (fig. 15 top) the vertical scale has been zoomed in order to show the almost exact preservation of the polarization. Unfortunately when going to  $1.5\sigma$ - $1.5\sigma$ - $1.5\sigma$  (fig. 15 bottom) about 30% polarization is lost. For  $2\sigma$ - $2\sigma$ - $2\sigma$  (fig. 16 top) there is large polarization loss already around 795 GeV. The “recovery” around 800 GeV has to be viewed with suspicion — it is an artifact of single particle tracking similar to the case of the ‘1b1b’ configuration. Finally at  $2.5\sigma$ - $2.5\sigma$ - $2.5\sigma$  (fig. 16 bottom) already the static polarization limit ( $P_{\text{lim}}$ ) is low. The polarization vanishes immediately after starting the ramp. Figure 17 shows the optimal scheme from filtering with the luminosity optics, ‘1d3c’. Although the configurations ‘3e1b’ and ‘1d3c’ look quite similar (North $\leftrightarrow$ South,  $\pm 67.5^\circ \leftrightarrow \pm 45^\circ$ ), the ‘1d3c’ totally fails with the separation optics. The polarization drops to roughly 20% even in the  $1\sigma$  case (top). On the  $1.5\sigma$ - $1.5\sigma$ - $1.5\sigma$  torus (bottom) the polarization seems to oscillate but a closer look at the data again shows that also the average spin direction is flipping at many additional resonances after crossing the major resonance at 803 GeV. Hence the oscillating polarization is again an artifact from single spin analysis. The results would be easier to interpret with a large spin ensemble. But that would increase computation time significantly.

HERA-P / "3e1b"

 =  $-V * H * SN_x^* H * V$



 =  $-V * H * SN_x^* H * V$

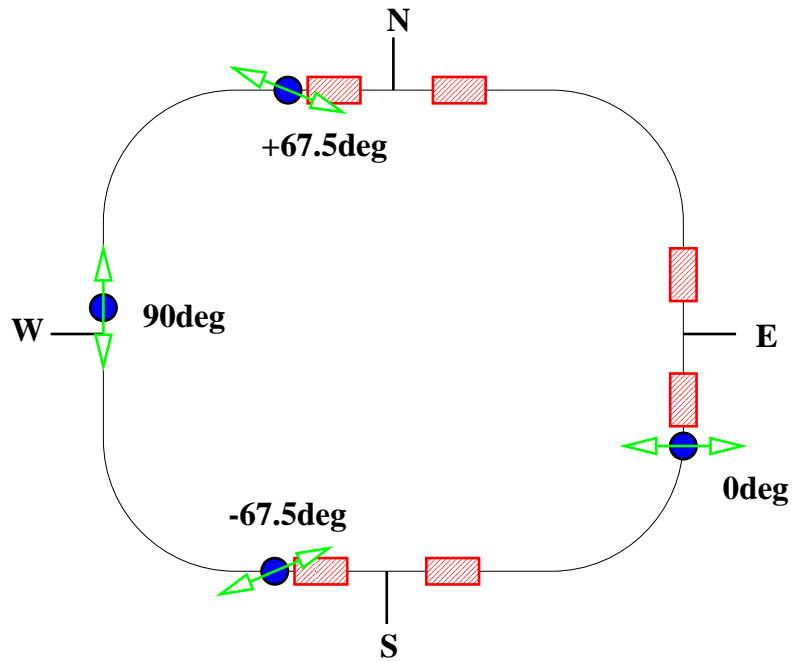


Figure 14: The snake schemes '3e1b' and '1d3c'

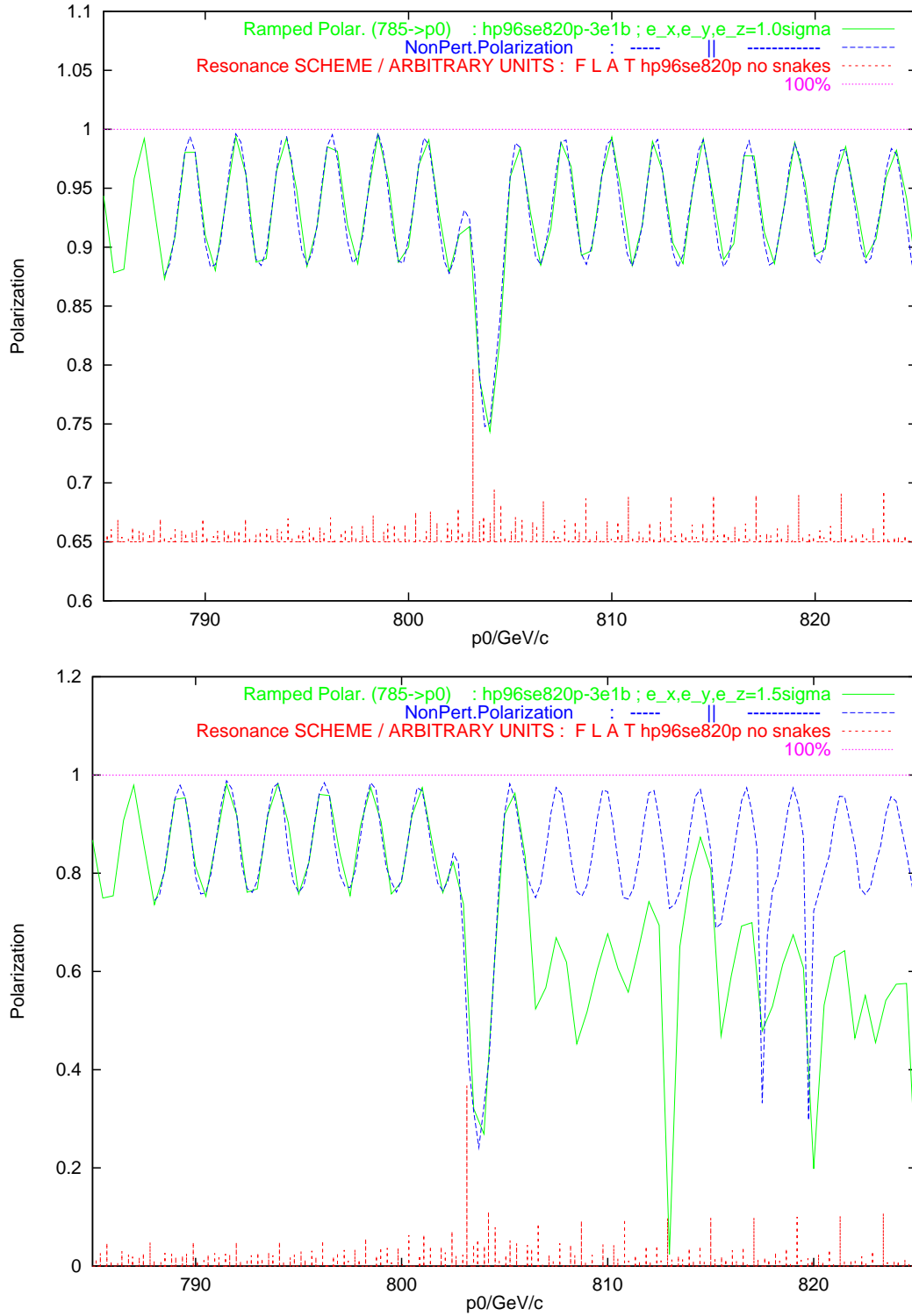


Figure 15: Scheme '3e1b': comparison between  $P_{(S)}$  and  $P_{lim}$  for 1.0 (top) and 1.5  $\sigma$  (bottom) in all 3 planes

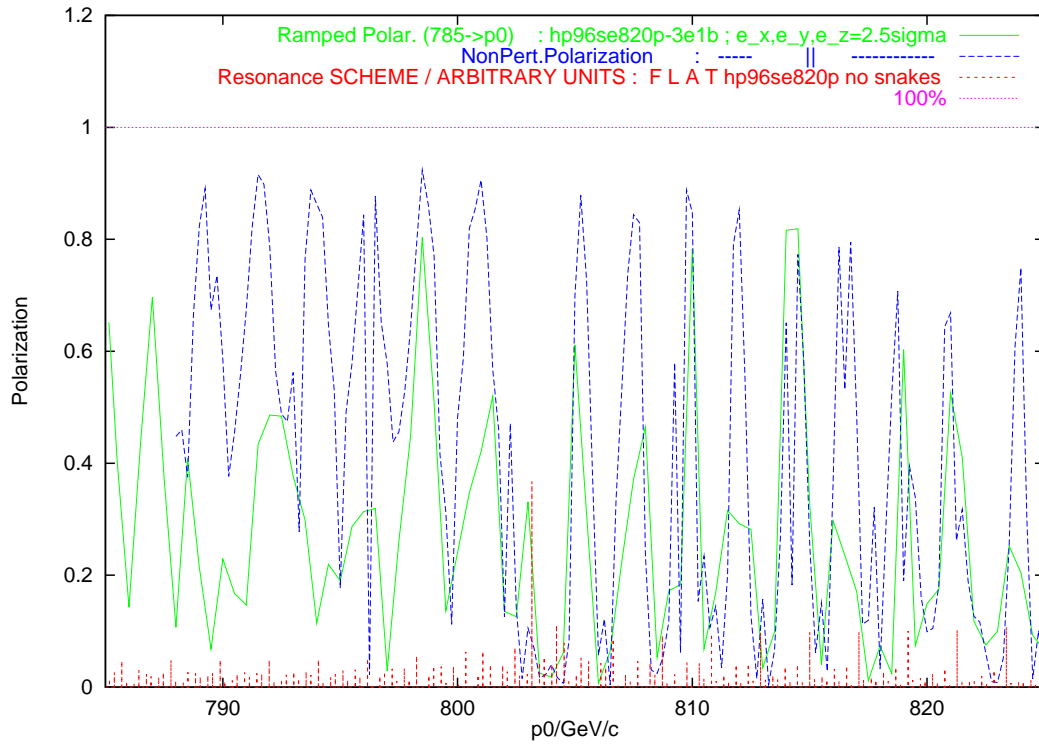
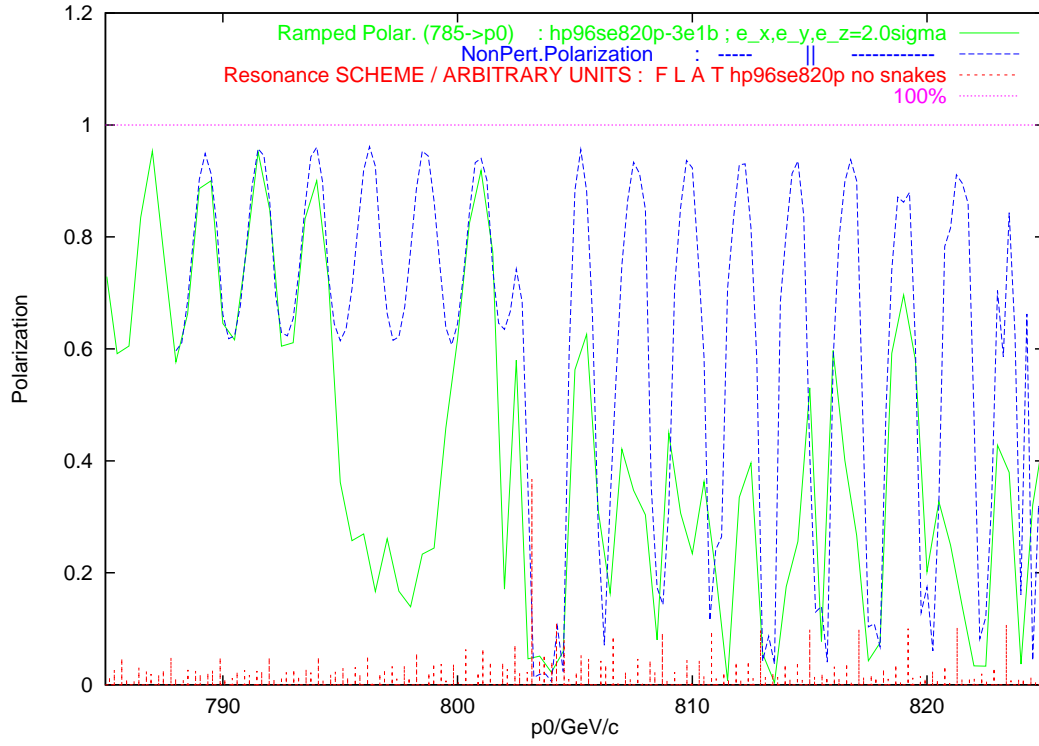


Figure 16: Scheme '3e1b': comparison between  $P_{(S)}$  and  $P_{lim}$  for 2.0 (top) and 2.5  $\sigma$  (bottom) in all 3 planes



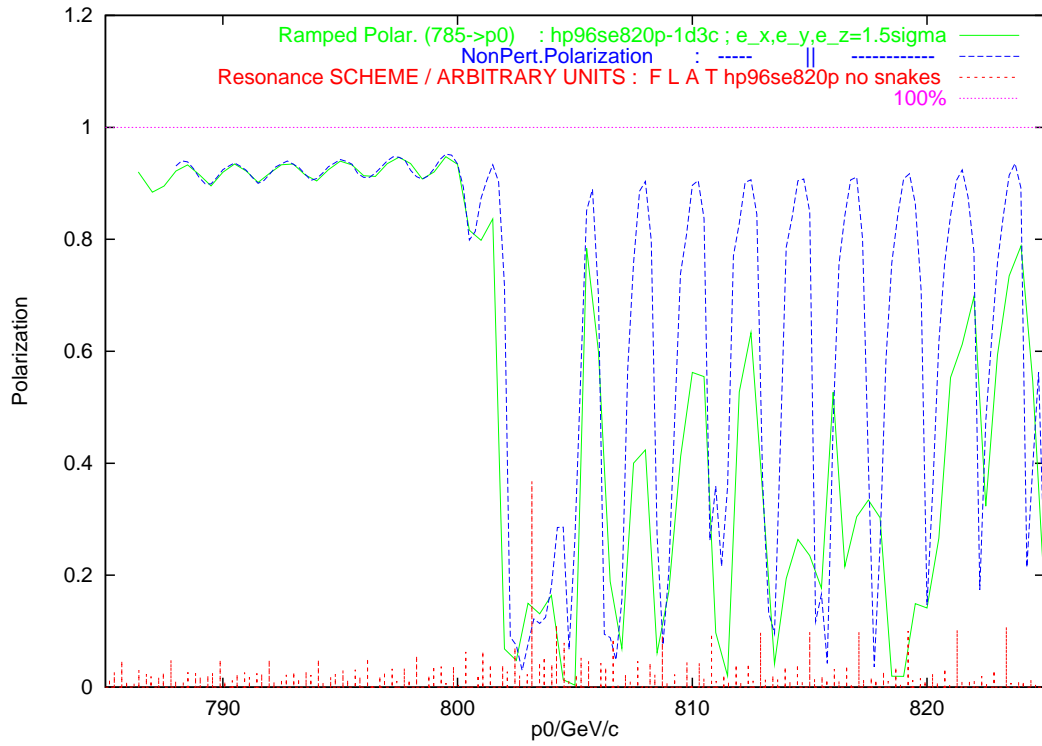
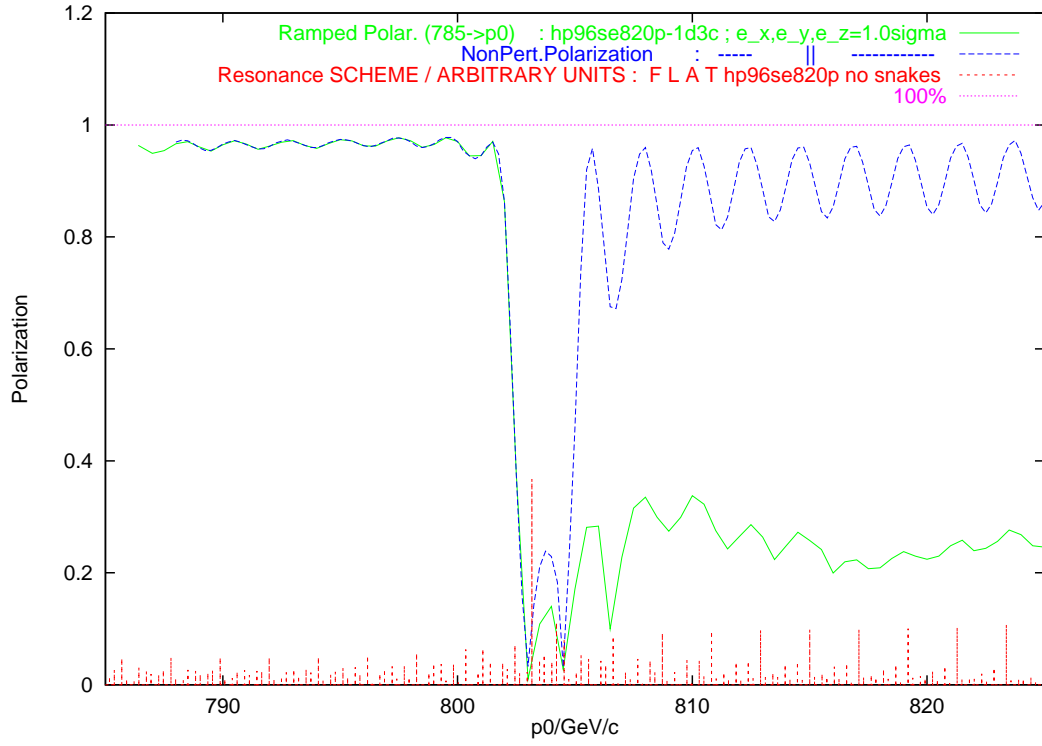


Figure 17: Scheme '1d3c': comparison between  $P_{(S)}$  and  $P_{lim}$  for 1.0 (top) and 1.5  $\sigma$  (bottom) in all 3 planes

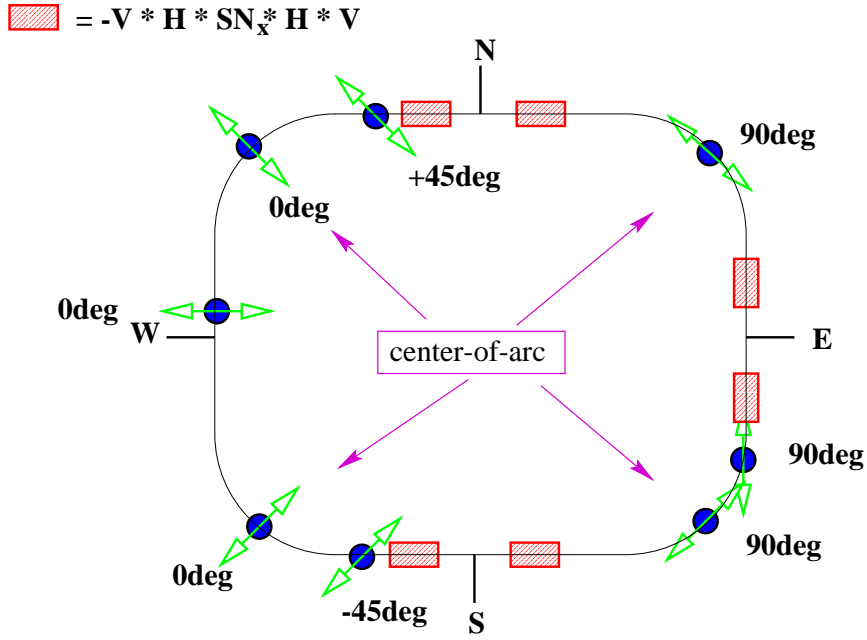


Figure 18: The snake schemes '33e111b3'

Figures 19 and 20 show the ramp simulation for the 8–snake scheme '33e111b'. It is obvious from figure 19 that in case of the  $1\sigma$ - $1\sigma$ - $1\sigma$  torus (top) the polarization is conserved for the full energy range of the simulation. The vertical axis of the upper plot has been zoomed. On the  $1.5\sigma$ - $1.5\sigma$ - $1.5\sigma$  torus (bottom) the polarization drops by 3%, but a few percent loss on the strongest resonance in the whole range of 40 to 820 GeV seems tolerable. In the  $2\sigma$  case (figure 20 top) there are already four steps at which losses occur *before* the 803 GeV region

1. a drop of ca. 5% directly at the beginning of the ramp,
2. around 792 GeV the polarization drops by ca. 20%,
3. around 796 GeV the polarization drops by another 40% and
4. around 800 GeV the polarization drops to 0.

Each of these is separated by 4 GeV. If we assume an intrinsic resonance structure width of  $\frac{m_p}{G} = 523$  MeV which is the separation of integer resonances if the ring was flat, then with a snake sequence of 8 per turn we generally observe [19] an approximate resonance period of 4 GeV. For  $2.5\sigma$ - $2.5\sigma$ - $2.5\sigma$  polarization vanishes immediately at the beginning of the ramp. Therefore it does not seem as if doubling the number of Siberian Snakes (not including the flatteners) doubles the beam width with acceptable spin stability. The largest stable torus with four snakes in the schemes '3e1d' and '3111' is  $1\sigma$  in all three planes corresponding to normalized emittances of  $\varepsilon_x^n = \varepsilon_y^n = 4\pi$  mm mrad and  $\varepsilon_z^n = 1.78 \cdot 10^4 \pi$  mm mrad (which means an energy spread of  $\pm 10^{-4}$ ). The largest stable torus with eight snakes ('33e111b3') is  $1.5\sigma$ - $1.5\sigma$ - $1.5\sigma$ , corresponding to  $\varepsilon_x^n = \varepsilon_y^n = 9\pi$  mm mrad and  $\varepsilon_z^n = 4.00 \cdot 10^4 \pi$  mm mrad.

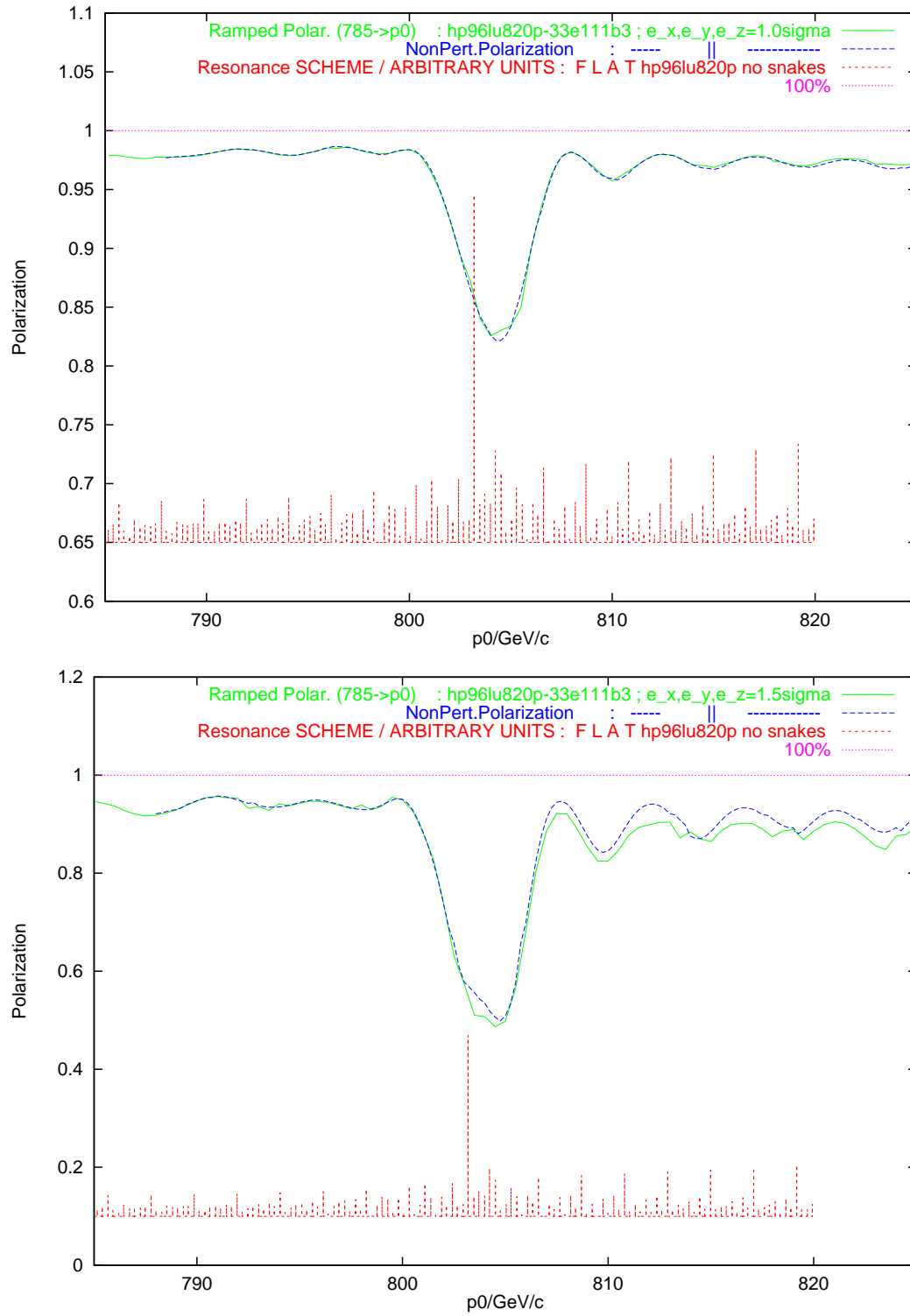


Figure 19: Scheme '33e111b3': comparison between  $P_{(s)}$  and  $P_{lim}$  for 1.0 (top) and 1.5  $\sigma$  (bottom) in all 3 planes

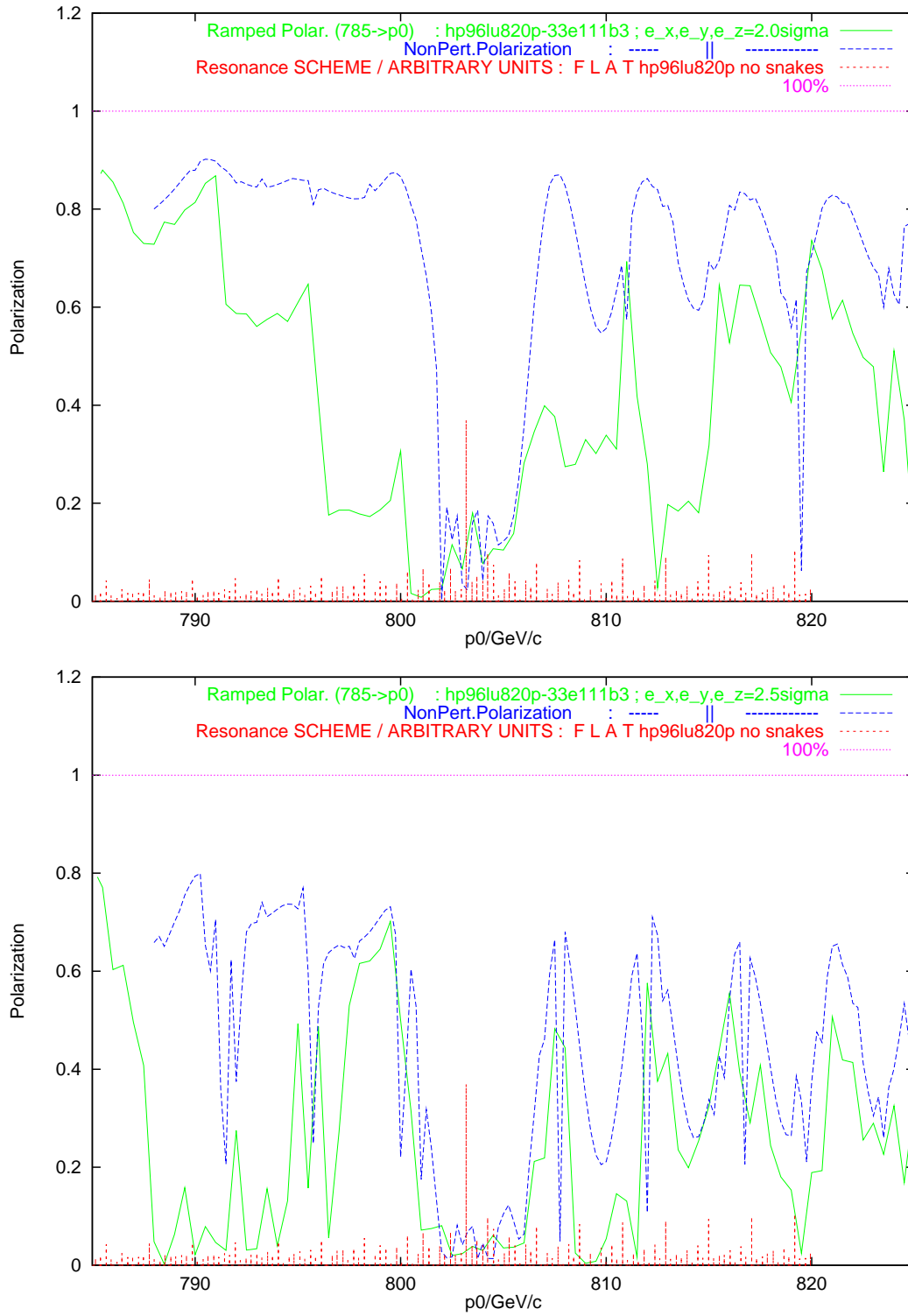


Figure 20: Scheme '33e111b3': comparison between  $P_{(s)}$  and  $P_{lim}$  for 2.0 (top) and 2.5  $\sigma$  (bottom) in all 3 planes

## 5 Conclusion

This report shows the power of the invariant spin field for studying polarization in high energy accelerators. It offers a consistent formulation for various phenomena observed in tracking simulations. So far *no* high energy accelerator runs with polarized protons so a practical proof of applicability still remains. Hopefully in the year 2000 the RHIC polarized proton runs will begin and first experimental results on spin stability can be obtained.

To summarize the results of the simulations for HERA-p we conclude the following:

- Modifications to the pre-accelerator chain will be necessary. Problems in the low and intermediate energy region, although considered less severe than at HERA are not fully analyzed yet.
- Crossing of the strongest resonant area at 803 GeV seems possible with negligible polarization losses only for the inner part of the beam (up to about 1 or 1.5  $\sigma$ ).
- The outer parts up to the 95% emittances are still critical.
  - The static polarization limit  $P_{\text{lim}}$  on the outer tori is low, typically 50% on  $2\sigma$ - $2\sigma$ - $2\sigma$  with 4-snakes schemes and up to 65% with the best 8-snake scheme ‘33e111b3’ [19].
  - The dynamic polarization  $P_{\text{dyn}}$  drops to zero even with the best schemes on the  $2\sigma$ - $2\sigma$ - $2\sigma$  torus when crossing 803 GeV.
- 8 snakes, *properly chosen*, seem to relax the situation slightly. But one can actually misuse the additional degrees of freedom to make an 8-snake scheme less efficient than a 4-snake scheme.
- It will be necessary to tune the optics of HERA-p in order to allow polarized proton operation.

In the future we will mainly have to work on the following subjects:

- Tuning of the optics at the resonant regions to conserve  $P_{\text{dyn}}$  and at the high energy working point to maximize  $P_{\text{lim}}$ .
- Our studies so far only take into account synchro-betatron motion in an undistorted machine. The final prove of feasibility has to include closed orbit distortions.
- spin stability under perturbations like noise, beam-beam effect, etc. have to be analyzed. The static invariant spin field  $\hat{n}(\vec{z}, l; \gamma_0)$  and the spin action  $\hat{S}_{\gamma_0} \cdot \hat{n}(\vec{z}, l; \gamma_0)$  seem to be the right starting points for perturbative expansions.
- non-linear orbital effects like chromaticity have to be taken into account.
- Even if stable operation is feasible with the ‘96 luminosity-optics at 820 GeV one still has to show whether polarization can be maintained with the “luminosity upgraded” HERA-p and/or at 920 GeV !

# References

- [1] *Proceedings of the 2nd topical Workshop on Deep Inelastic Scattering of Polarized Targets: Theory meets Experiment* IfH Zeuthen (1997)
- [2] D.P.Barber, *Proceedings of the Workshop on Prospects of Spin Physics at HERA* , IfH Zeuthen (1995)
- [3] L.H.Thomas, *Phil.Mag.* **3**, 1 (1927) ;  
V.Bargman, L.Michel, V.L.Telegdi, *Phys. Rev. Lett.* **2**, 435 (1959)
- [4] K.Yokoya, DESY preprint DESY 86-057 (1986)
- [5] V.Balandin, N.Golubeva, DESY internal report M-96-04 (1996)
- [6] G.H.Hoffstätter, M.Vogt, *SPRINT User's Guide and Reference Manual (vers. 0.9)* to appear soon
- [7] K.Heinemann, DESY preprint DESY 97-166
- [8] S.R.Mane, FERMILAB technical report TM-1515 (1988)
- [9] K.Heinemann, G.H.Hoffstätter, *Phys. Rev.* **E54**, 4240 (1996)  
or: DESY preprint DESY 96-078 (1996)
- [10] S.Y.Lee, *Spin Dynamics and Snakes in Synchrotrons*, (World Scientific Publishing Co. Pte.Ltd, 1997)
- [11] M.Froissart, R.Stora, *Nucl. Inst. Meth.* **7**, 297 (1960)
- [12] G.H.Hoffstätter, DESY Beschleuniger Betriebsseminar 1996 HERA-report 96-05, 477 (1996)
- [13] J.Ellison, G.H.Hoffstätter, to be published
- [14] The Spin Collaboration, The DESY Polarization Team, *Acceleration of Polarized Protons to 820 GeV at HERA* , University of Michigan report UM HE 96-20 (1996)
- [15] T.Roser, Polarized Proton Beams *Proceedings of the 1995 IEEE Particle Accelerator Conference and International Conference on High-Energy Accelerators*, 3154 (1996) ;  
M.Bai, et al., *Phys. Rev.* **E**,5 (1997)
- [16] G.H.Hoffstätter, D.P.Barber, M.Vogt, *Proceedings of the 1997 workshop on 'Non-linear and Stochastic Beam Dynamics in Accelerators' in Lüneburg*, DESY preprint DESY 97-161 (1997)
- [17] Ya.Derbenev, private communication
- [18] K.Steffen, DESY preprint DESY 88-068 (1988)
- [19] D.P.Barber, G.H.Hoffstätter, M.Vogt, in preparation
- [20] Ya.Derbenev, University of Michigan preprint UM HE 97-07